

AD-A265 275



AFOSR-TR- 83 0081

2



Department of Mechanical and Aerospace Engineering  
Rutgers University  
P. O. Box 909  
Piscataway, NJ 08855

Report RU-TR-MAE-184-F

*Theoretical Investigation of 3-D Shock Wave - Turbulent  
Boundary Layer Interactions*

Doyle D. Knight

Interim Report for Period 1 March 1992 to 30 September 1992  
Approved for Public Release - Distribution Unlimited

Air Force Office of Scientific Research  
Building 410  
Bolling AFB  
Washington, DC 20332

November 1992

DISTRIBUTION STATEMENT A  
Approved for public release  
Distribution Unlimited

DTIC  
ELECTE  
JUN 0 1 1993  
S B D

# DISCLAIMER NOTICE



THIS DOCUMENT IS BEST QUALITY AVAILABLE. THE COPY FURNISHED TO DTIC CONTAINED A SIGNIFICANT NUMBER OF COLOR PAGES WHICH DO NOT REPRODUCE LEGIBLY ON BLACK AND WHITE MICROFICHE.

6c. ADDRESS (City, State, and ZIP Code) P.O.Box 909, Piscataway, NJ 08855-0909	7b ADDRESS (City, State, and ZIP Code) Bldg. 410, Bolling AFB Washington DC 20332
---	---

8a. NAME OF FUNDING / SPONSORING ORGANIZATION Air Force Office of Sc. Res.	8b. OFFICE SYMBOL (if applicable) AFOSR/NA	9. PROCUREMENT INSTRUMENT IDENTIFICATION NUMBER AFOSR-86-0266
---	---	--

8c. ADDRESS (City, State, and ZIP Code) Bldg. 410, Bolling AFB Washington DC 20332	10. SOURCE OF FUNDING NUMBERS		
	PROGRAM ELEMENT NO. 230TTA1	PROJECT NO. 2307	TASK NO. A1

11. TITLE (Include Security Classification) **61102F**  
Theoretical Investigation of 3-D Shock Wave-Turbulent Boundary Layer Interactions

12. PERSONAL AUTHOR(S)  
Doyle D. Knight

13a. TYPE OF REPORT Interim	13b. TIME COVERED FROM 92/03/1 TO 92/09/30	14. DATE OF REPORT (Year, Month, Day) 93/11/30	15. PAGE COUNT 56
--------------------------------	---	---	----------------------

16. SUPPLEMENTARY NOTATION

17. COSATI CODES	18. SUBJECT TERMS (Continue on reverse if necessary and identify by block number) High speed flows; shock/boundary layer interactions; computational fluid dynamics; Navier-Stokes; turbulence
FIELD	
GROUP	
SUB-GROUP	

19. ABSTRACT (Continue on reverse if necessary and identify by block number)

The research concerns the understanding of 3-D shock wave/turbulent boundary layer interactions. The research effort during the current period focused on the following areas:

(a) the 3-D double fin ("crossing shock") interaction at Mach 8.3 for symmetric 15° fins, (b) the 3-D crossing shock interaction at Mach 4 for symmetric 15° fins, and (c) the 3-D triple fin ("triple shock") interaction at Mach 8.3 for 10° fins.

The principal conclusions of the research effort are presented below:

(...continued on next page)

**93-12238**  
93 5 20 000

20. DISTRIBUTION / AVAILABILITY OF ABSTRACT <input type="checkbox"/> UNCLASSIFIED/UNLIMITED <input type="checkbox"/> SAME AS RPT. <input type="checkbox"/> DTIC USERS	21. ABSTRACT SECURITY CLASSIFICATION Unclassified
--	--

22a. NAME OF RESPONSIBLE INDIVIDUAL DR Lomida Labell	22b. TELEPHONE (Include Area Code) 202-767-4935	22c. OFFICE SYMBOL AFOSR / NA
---	--	----------------------------------

(... continued from Block 19)

1. Computed results for the Mach 8.3 crossing shock interaction for 15° fins using the Baldwin-Lomax and Rodi turbulence models display similar results for surface pressure and pitot pressure and yaw angle profiles in the flow. The computed results show generally good agreement with experiment. Surface heat transfer is not predicted accurately by either computation, indicating a need for more accurate turbulence models. The principal feature of the streamline structure of the flowfield is the formation of a low total pressure jet comprising two helical counter rotating vortices. This jet structure is stronger (larger) than in the 10° interaction examined previously at the same Mach number. The wave structure of the interaction consists of a complex system of shock wave and expansion fan patterns and is generally similar to that observed in supersonic crossing shock interactions.
2. The computed and experimental flowfield wave structures for the Mach 4, 15° fin crossing shock interaction show good overall agreement. The computed results provide additional information regarding wave and streamline structures not observed in the experiment. The computed and experimental wave structures differ in one aspect: a segment of the reflected shock structure downstream of the crossed shocks observed in the experiment is absent in the computation. The computed and experimental surface flow patterns show generally good agreement. The principal feature of the flowfield streamline structure is the formation of a low total pressure jet comprising two weakly counter rotating helical vortices, and is similar to that observed for the Mach 8.3 case.
3. A preliminary analysis of the computed results for the 3-D triple shock interaction at Mach 8.3 for 10° fins indicates a very complex flowfield structure. The principal feature of the streamline structure is the formation of two distinct regions of low total pressure, one adjacent to the flat plate and the other adjacent to the top wedge (fin). Each of these two low total pressure regions comprise two counter rotating vortical structures. Further analysis of the computed results is in progress.

<b>Accession For</b>	
NTIS CRA&I	<input checked="" type="checkbox"/>
DTIC TAB	<input type="checkbox"/>
Unannounced	<input type="checkbox"/>
Justification	
By	
Distribution/	
Availability Codes	
Dist	Avail and/or Special
A-1	

## Preface

This report presents the research accomplishments for the program entitled "Theoretical Investigation of Three - Dimensional Shock Wave / Turbulent Boundary Layer Interactions" for the period 1 March 1992 through 30 September 1992.

Over this time period, the research program involved a series of collaborative theoretical (computational) and experimental investigations of 3-D multiple intersecting shock wave / turbulent boundary layer interactions ("3-D turbulent interactions"). The primary focus of the research effort was the interaction generated by double fin ("crossing shock") configurations for supersonic and hypersonic flow conditions. The theoretical model in the computations is the full 3-D mean compressible Reynolds-averaged Navier-Stokes (RANS) equations incorporating turbulence effects through the algebraic eddy viscosity model of Baldwin and Lomax. In addition to the above studies of the crossing shock problem, a computational study of the 3-D hypersonic turbulent interaction due to a triple fin ("triple shock") configuration was completed.

The assistance of the following individuals during various stages of the research effort is appreciated: Dr. L. Sakell (Air Force Office of Scientific Research), E. Pegot (NASA - Ames Research Center), W. Kish, R. B. Thomas and J. Salowe (Rutgers University - SRAC). The research effort also benefited from the scientific interactions with Dr. G. Settles and Mr. T. Garrison (Pennsylvania State University) and Dr. C. C. Horstman (NASA - Ames Research Center).

# Contents

I. Objectives . . . . .	4
II. Status of Research Program . . . . .	4
III. Research Accomplishments : 1 March 1992 - 30 September 1992 . . . . .	7
A. 3-D crossing shock interaction at Mach 8.3 . . . . .	7
B. 3-D crossing shock interaction at Mach 4 . . . . .	9
C. 3-D triple shock interaction at Mach 8.3 . . . . .	11
IV. Research program for the period : 1 October 1992 - 30 September 1993 . . . . .	16
V. References . . . . .	17
VI. Visitors to Rutgers University : 1 March 1992 - 30 September 1992 . . . . .	18
VII. Archival papers : 1 March 1992 - 30 September 1992 . . . . .	18
VIII. Videotapes: 1 March 1992 - 30 September 1992 . . . . .	19
IX. Conference papers: 1 March 1992 - 30 September 1992 . . . . .	19
X. Papers in review : 1 March 1992 - 30 September 1992 . . . . .	20
XI. Presentations : 1 March 1992 - 30 September 1992 . . . . .	20
XII. List of personnel and degrees awarded : 1 March 1992 - 30 September 1992 . . . . .	20
A. List of personnel . . . . .	20
B. Degrees awarded . . . . .	21
XIII. List of attached papers . . . . .	21

## I. Objectives

The principal objective of the overall research program is to further the understanding of 3-D shock wave / turbulent boundary layer interactions ("3-D turbulent interactions") through a synthesis of the following specific goals, namely, (a) the development and validation of theoretical models for 3-D turbulent interactions, (b) the determination of the flowfield structure of 3-D turbulent interactions for specific geometries, (c) the investigation of methods of control and modification of 3-D turbulent interactions and (d) the development of a unified understanding of the flowfield structure of 3-D turbulent interactions. A brief discussion of the status of the research program is provided in the following section.

## II. Status of Research Program

Significant progress has been made in achieving the aforementioned objectives. Over the past few years, the principal focus of the research effort has been the understanding of the flowfield structure of complex 3-D turbulent interactions such as that generated due to supersonic/hypersonic flow past double fin ("crossing shock") configurations (Fig.1). Such interactions find practical application in the design of air-breathing inlets for aerospace vehicles (e.g., the National Aerospace Plane (NASP) (VanWie *et al.* 1990))<sup>1</sup>. The research effort has involved close collaboration between theory (computation) and experiment and has been successful in identifying and understanding several key features of the overall mean flowfield structure of 3-D crossing shock interactions.

The theoretical model in the above 3-D crossing shock interaction studies is the full three-dimensional mean compressible Reynolds-averaged Navier-Stokes (RANS) equations (Rubesin and Rose 1973) incorporating the algebraic turbulent eddy viscosity model of Baldwin and Lomax (1978). The governing equations are solved using a highly efficient hybrid explicit-implicit algorithm developed by Knight (1984). The interactions have been studied for a range of Mach numbers (Mach 3 to 8.3) and fin angles ( $\alpha = 9^\circ$  to  $15^\circ$ ).

---

<sup>1</sup>References are provided in Section V.

The principal feature of the streamline structure of these interactions is observed to be the presence of a large low total pressure jet comprising two counter-rotating helical vortices. The vortices are formed due to the individual single fin generated shock wave/boundary layer interactions (Knight *et al.* 1987, 1992). This streamline structure is complemented by a complex wave structure involving the interaction of the lambda ( $\lambda$ ) shaped shock structure associated with each separation vortex.

In addition to the above 3-D crossing shock interaction studies, the research effort has recently focused on the more complex 3-D symmetric triple fin ("triple shock") interaction (Fig.2) in hypersonic flow. The interaction for Mach 8.3 and  $\alpha = 10^\circ$  fins has been examined computationally using the same theoretical model as employed in the crossing shock studies, namely, the 3-D RANS equations together with the Baldwin-Lomax turbulence model. A preliminary examination of the computed results has revealed an extremely complex three dimensional interaction. Increased understanding of the flowfield structure (through further theoretical and experimental examinations) has significant potential for the improved design of high speed inlet systems.

The specific accomplishments of the research program over the period 1 March 1992 through 30 September 1992 are described in Section III of this report. The future focus of the research program for the period 1 October 1992 through 30 September 1993 is outlined in Section IV. A key element of the overall research program is the extensive scientific collaboration between the author and Dr. C. C. Horstman (NASA - Ames Research Center) and Prof. G. Settles (Pennsylvania State University). Additional collaborations with Prof. D. Dolling (University of Texas), Prof. S. M. Bogdonoff and Prof. A. Smits (Princeton University) and Dr. A. Zheltovodov (ITPM, Russia) are expected to continue.

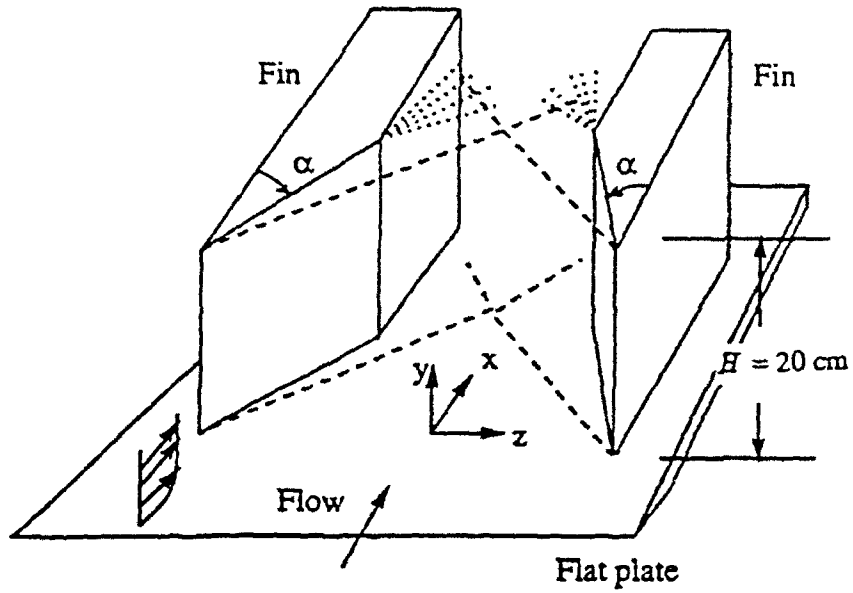


Fig.1 3-D crossing shock configuration

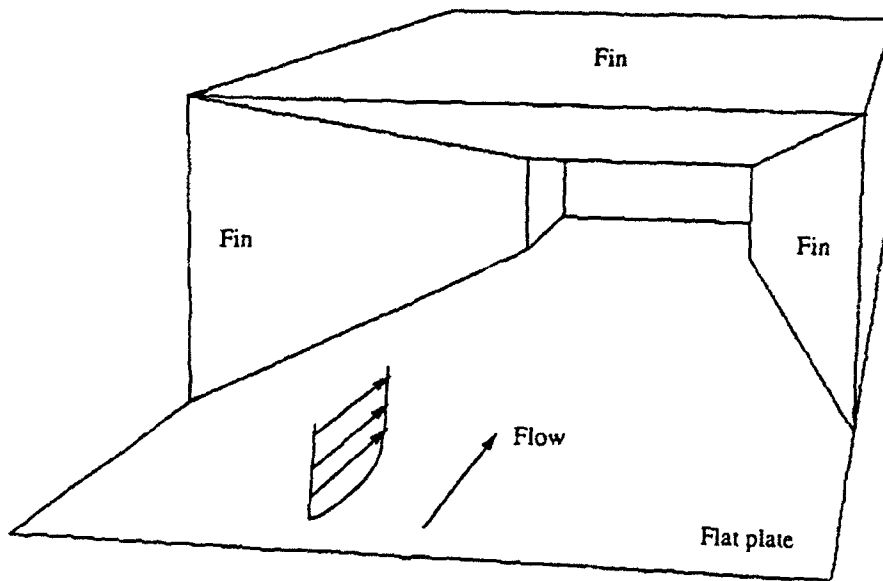


Fig.2 3-D triple shock configuration

### **III. Research Accomplishments : 1 March 1992 - 30 September 1992**

The research program during the period 1 March 1992 through 30 September 1992 followed the specific objectives outlined in Section I. The accomplishments during the above time period are discussed below in Sections A - C. The principal focus of the research effort was the understanding of the 3-D "crossing shock" turbulent interaction generated due to supersonic/hypersonic flow past double fin configurations, relevant to high speed inlet design. Full details of the research activity may be found in the attached conference papers (see Section XIII).

An important aspect of the research effort was the close scientific collaboration of the principal investigator with the computational and experimental research of Dr. C. C. Horstman (NASA - Ames Research Center) and the experimental research of Prof. G. S. Settles (Pennsylvania State University). Specifically, computations were performed by the principal investigator and his students and the results compared with the experimental data of Settles for a supersonic crossing shock interaction at Mach 4. Also, a computation was performed for a crossing shock interaction at Mach 8.3 and the results compared with separate computational results of Horstman and experimental results of Kussoy and Horstman (1992). This collaborative effort is a continuing element of the overall research program.

#### **A. 3-D crossing shock interaction at Mach 8.3**

The recent focus of the national aerospace industry towards building supersonic high speed civil transport (HSCT) and the hypersonic National Aerospace Plane (NASP) (VanWie 1990) has led to renewed interest in the aerodynamic phenomenon of 3-D multiple intersecting shock wave / turbulent boundary layer interactions. A clear understanding of such interactions is critical to the efficient design of propulsion systems for aerospace vehicles. Complex 3-D turbulent interactions within the inlet portion of the propulsive system may lead to flow separation and consequently high drag and increased aerodynamic heating - phenomena that may be detrimental to engine operation and performance.

The present research effort focused on the 3-D crossing shock interaction due to the flow past a shock generator geometry (Fig.1) that is a simplified abstraction of a real hypersonic inlet. The geometry comprises two opposing sharp fins, each of angle  $\alpha$ , mounted on a flat plate. The hypersonic flow past the geometry generates oblique shocks from the leading edges of the fins. These shocks interact with each other and with the turbulent boundary layer on the flat plate.

During the present research period, the 3-D crossing shock interaction due to symmetric  $\alpha = 15^\circ$  fins at a Mach number of 8.3, Reynolds number  $Re_{\delta_\infty} = 1.7 \times 10^5$  and wall temperature  $T_w = 0.3 T_{adiabatic}$  was investigated theoretically (computationally). This interaction is the strongest 3-D crossing shock interaction studied to date (the overall inviscid pressure rise is 45). An earlier research effort by the principal investigator and his students examined the interaction due to  $\alpha = 10^\circ$  fins at Mach 8.3, corresponding to an overall inviscid pressure rise of 19.5, and the results were reported in Narayanswami *et al.* (1992). The computed results in the present study were compared with separate computational results of Horstman and with the experimental measurements of Kussoy and Horstman (1992). The theoretical model in both computations was the full 3-D mean compressible Reynolds-averaged Navier-Stokes (RANS) equations. The computations of the author incorporated the algebraic turbulent eddy viscosity model of Baldwin and Lomax. The computations of Horstman incorporated the two equation (modified  $k-\epsilon$ ) turbulence model of Rodi (1991). Full details of the combined theoretical-experimental investigation are provided in the AIAA Paper No. 93-0779 to be presented at the 31st Aerospace Sciences Meeting, January 11-14, 1993, Reno, NV (see Section XIII, Attachment 1).

The principal conclusions of the study are summarized below:

- The computed results for flat plate surface pressure and for profiles of pitot pressure and yaw angle in the flowfield are similar for both the Baldwin-Lomax and Rodi turbulence models. The computed results show generally good agreement with experiment. Surface heat transfer is not predicted accurately by either computation, indicating a need for more accurate turbulence models.

- The overall flowfield structure is similar to that observed at lower (supersonic) Mach numbers. The principal feature of the streamline structure determined from particle traces (Fig.3) is the formation of a low total pressure jet comprising two helical counter rotating vortices. This jet structure is stronger (larger) than in the  $\alpha = 10^\circ$  interaction examined previously at the same Mach number and occupies a significant portion of the outflow area between the fins. This significant flow separation and distortion has important implications to the design of hypersonic inlets.
- The wave structure of the interaction consists of a complex system of shock wave and expansion fan patterns (Fig.4), and is generally similar to that observed for supersonic crossing shock interactions.

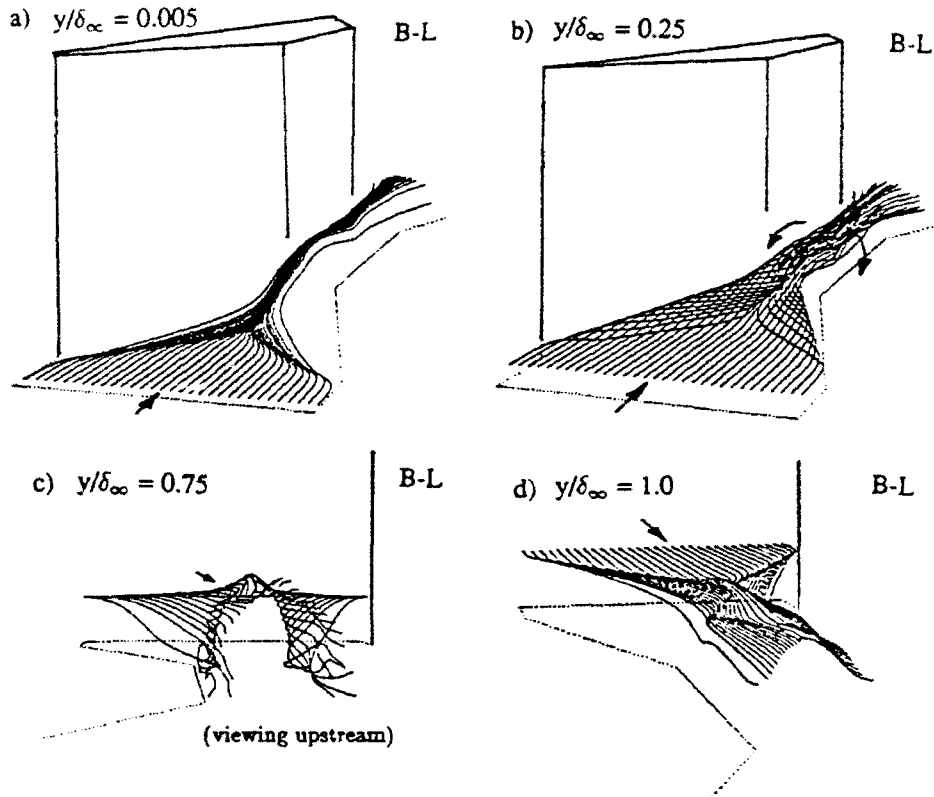


Fig.3 Computed streamline structure of Mach 8.3,  $\alpha = 15^\circ$  crossing shock interaction; particle traces originating from various  $y/\delta_\infty$  locations within the upstream boundary layer

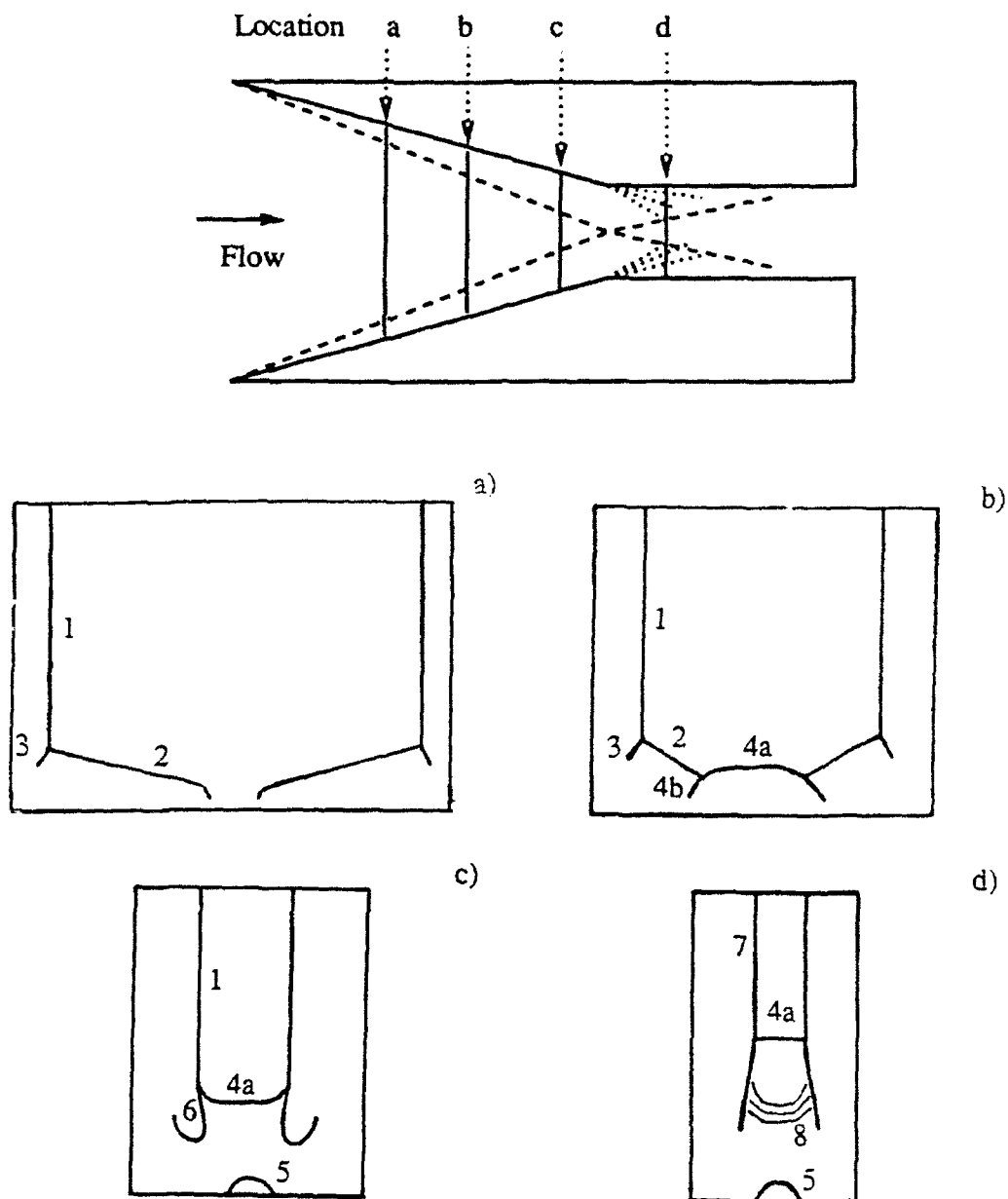


Fig.4 Computed wave structure of Mach 8.3,  $\alpha = 15^\circ$  crossing shock interaction (schematic) derived from static pressure contours on cross flow planes at locations a,b,c,d. Legend: 1 = primary shock, 2 = separation shock, 3 = rear shock, 4 (a,b) = conical shock, 5 = shock, 6 = high pressure region due to intersection of shocks 3 and 4b, 7 = reflected shock, 8 = expansion fan

## B. 3-D crossing shock interaction at Mach 4

The 3-D crossing shock interaction (Fig.1) for symmetric fins of angle  $\alpha = 15^\circ$  at Mach 3.83, Reynolds number  $Re_{\delta_\infty} = 2.7 \times 10^5$  and adiabatic walls was studied theoretically (computationally) in collaboration with the experimental effort led by Prof. G. S. Settles (Pennsylvania State University). The overall inviscid pressure rise is 9.5. The theoretical model is the full 3-D mean compressible RANS equations in conjunction with the algebraic turbulent eddy viscosity model of Baldwin and Lomax.

The overall flowfield structure of the interaction (Figs.5,6) was determined through a synthesis of the computed and experimental results. Experimental laser light sheet images at several streamwise locations provided the first direct look at the wave structure in a 3-D crossing shock interaction. The results confirmed the physical model of the flowfield proposed by Narayanswami *et al.* (1992) based on previous collaborative crossing shock studies at Mach 3. The computational results provided insight into the streamline structure of the interaction and provided additional wave structure information not observed in the experiment. The wave structure in the computation was determined through an examination of static pressure distributions on cross flow planes at several streamwise locations. Full details of the combined theoretical-experimental investigation are provided in the AIAA Paper No. 92-3670, presented at the AIAA/SAE/ASME/ASEE 28th Joint Propulsion Conference, July 6-8, 1992, Nashville, TN (see Section XIII, Attachment 2).

The principal conclusions of the study are:

- The computed and experimental flowfield wave structures showed good overall agreement. The computed results provided additional information regarding wave and streamline structures not observed in the experiment. The computed and experimental wave structures differed only in one aspect: a segment of the reflected shock structure downstream of the crossed shocks observed in the experiment was absent in the computation. The computed and experimental surface flow patterns showed general agreement.
- The principal feature of the streamline structure is the formation of a low total pressure jet (comprising two weakly counter rotating helical vortices) and is similar to that observed in hypersonic crossing shock interactions.

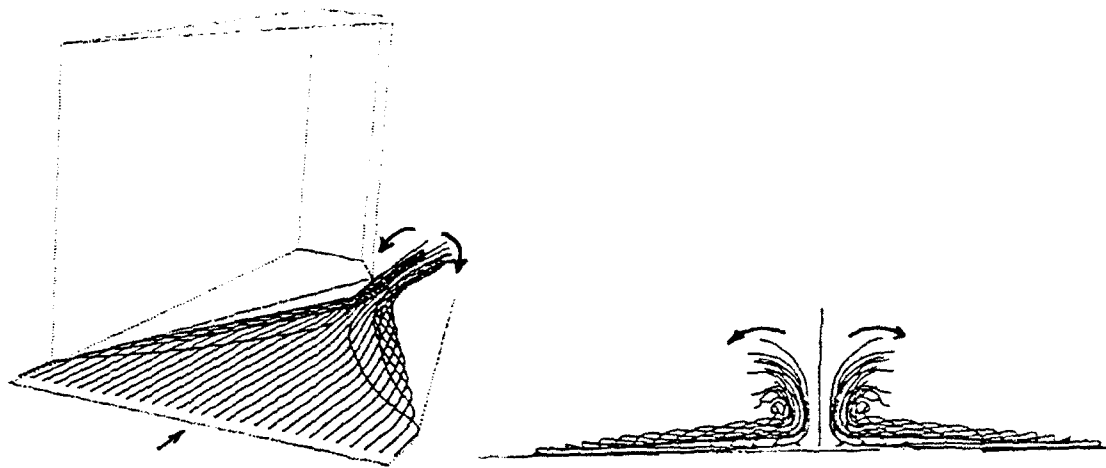


Fig.5 Computed streamline structure of Mach 4,  $\alpha = 15^\circ$  crossing shock interaction; particle traces originating from  $y/\delta_\infty = 0.25$  in the upstream boundary layer

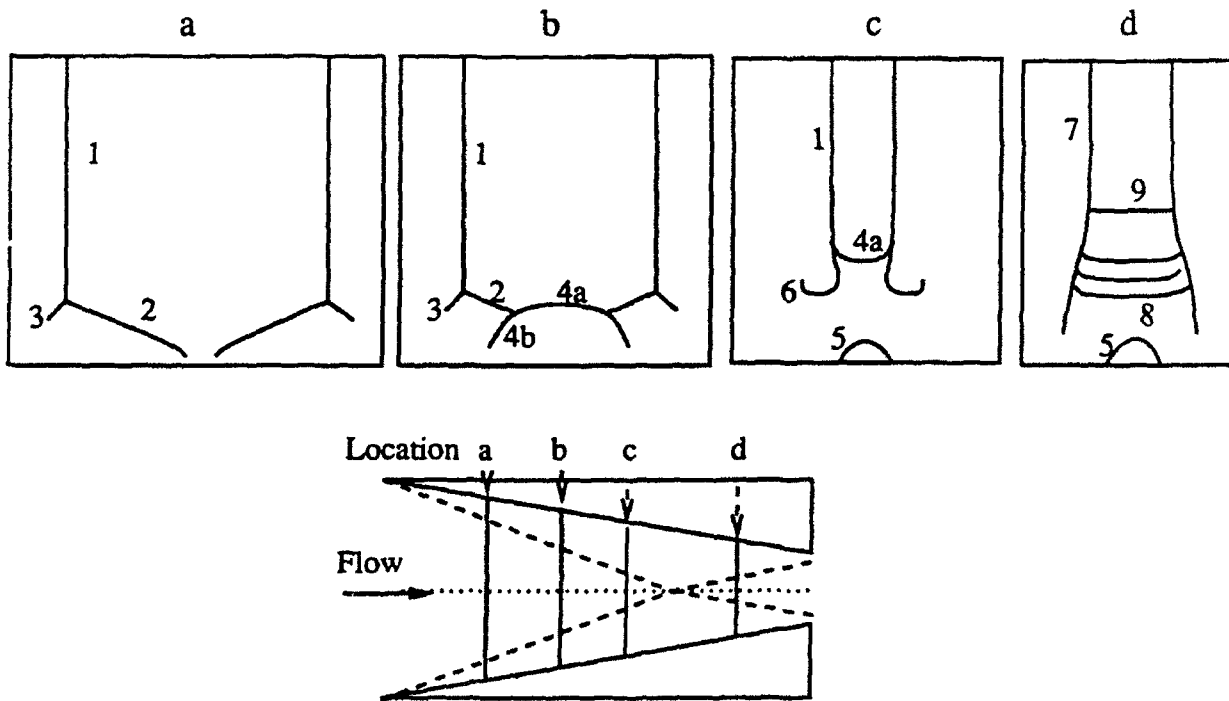


Fig.6 Computed wave structure (schematic) of Mach 4,  $\alpha = 15^\circ$  crossing shock interaction determined from static pressure contours on cross flow planes at locations a,b,c and d. Legend: 1 = primary shock, 2 = separation shock, 3 = rear shock, 4 (a,b) = conical shock, 5 = shock, 6 = high pressure region due to intersection of shocks 3 and 4b, 7 = reflected shock, 8 = expansion fan, 9 = shock

### C. 3-D triple shock interaction at Mach 8.3

A 3-D triple shock wave/turbulent boundary layer interaction ("3-D triple shock interaction") was examined theoretically (computationally). The triple shock generator geometry (Fig.2) is a more realistic representation of a typical hypersonic inlet than the crossing shock geometry (Fig.1). It includes a third sharp fin (wedge) at the top in addition to the two side fins of the crossing shock geometry. The hypersonic flow past the configuration causes oblique shocks to be generated from the leading edges of the two side fins and the top wedge. The complex three dimensional flowfield resulting from the interaction of the three shocks with the flat plate turbulent boundary layer is the focus of the research effort.

The flow conditions for the computation were chosen to coincide with experiments scheduled for July 1993 at the NASA-Ames Research Center by Drs. M. Kussoy and C. C. Horstman. The shock generator geometry involves fin angles of  $\alpha = 10^\circ$  for all three compression surfaces. The freestream Mach number is 8.3 and the Reynolds number  $Re_{\delta_\infty} = 1.7 \times 10^5$  (based on an estimated upstream boundary layer thickness of  $\delta_\infty = 3.25$  cm). The wall temperature is fixed at  $T_w = 0.3 T_{adiabatic}$ . The ratio of the side fin height (H) to boundary layer thickness  $\delta_\infty$  is 2.83. The aspect ratio (ratio of side fin height to side fin separation distance at the leading edge location) is 0.46.

The theoretical model is the full 3-D mean compressible RANS equations incorporating the algebraic turbulent eddy viscosity model of Baldwin and Lomax (1978). The solution of the governing equations was carried out using the hybrid explicit-implicit algorithm of Knight (1984). A grid of  $72 \times 60 \times 35$  points was employed, with the grid spacings based on grid resolution studies performed previously in 3-D crossing shock investigations (Narayanswami *et al.*, 1992). The governing equations were integrated to approximately  $5.8 T_c$  for convergence where  $T_c$  represents the characteristic time of the flow and is defined as the time taken by a fluid parcel to travel the length of the computational domain in the freestream.

A preliminary analysis of the computed results indicates a very complex 3-D interaction and shows significant deviation of the flowfield structure from the physical models developed for 3-D hypersonic crossing shock interactions. Fig.7 shows the total pressure distribution on cross flow planes at the location of the fin leading edge and at the outflow boundary. The formation of two distinct regions of low total pressure (denoted by "1" and "2") at the outflow is evident. The low total pressure region 1 is formed due to the crossing shock interaction on the flat plate. This structure is consistent with that observed in previous crossing shock interaction studies (Narayanswami *et al.*, 1992) at Mach 8.3. The low total pressure region 2 near the top fin surface is formed due to a second crossing shock interaction. The crossing shocks in this case are the shock segments oblique to the side fin surfaces formed by the local "corner" interactions (Shang *et al.* 1979). This region is smaller in size than region 1 primarily due to the relative thinness of the boundary layer developing on the top fin surface as compared to the flat plate boundary layer. Each of these low total pressure regions comprises two counter rotating helical vortices as seen from the streamline structure of the interaction shown in Fig.8.

Further analysis of the computed results is in progress. The computed results will be validated by comparison with the experiment measurements (currently scheduled for July 1993).

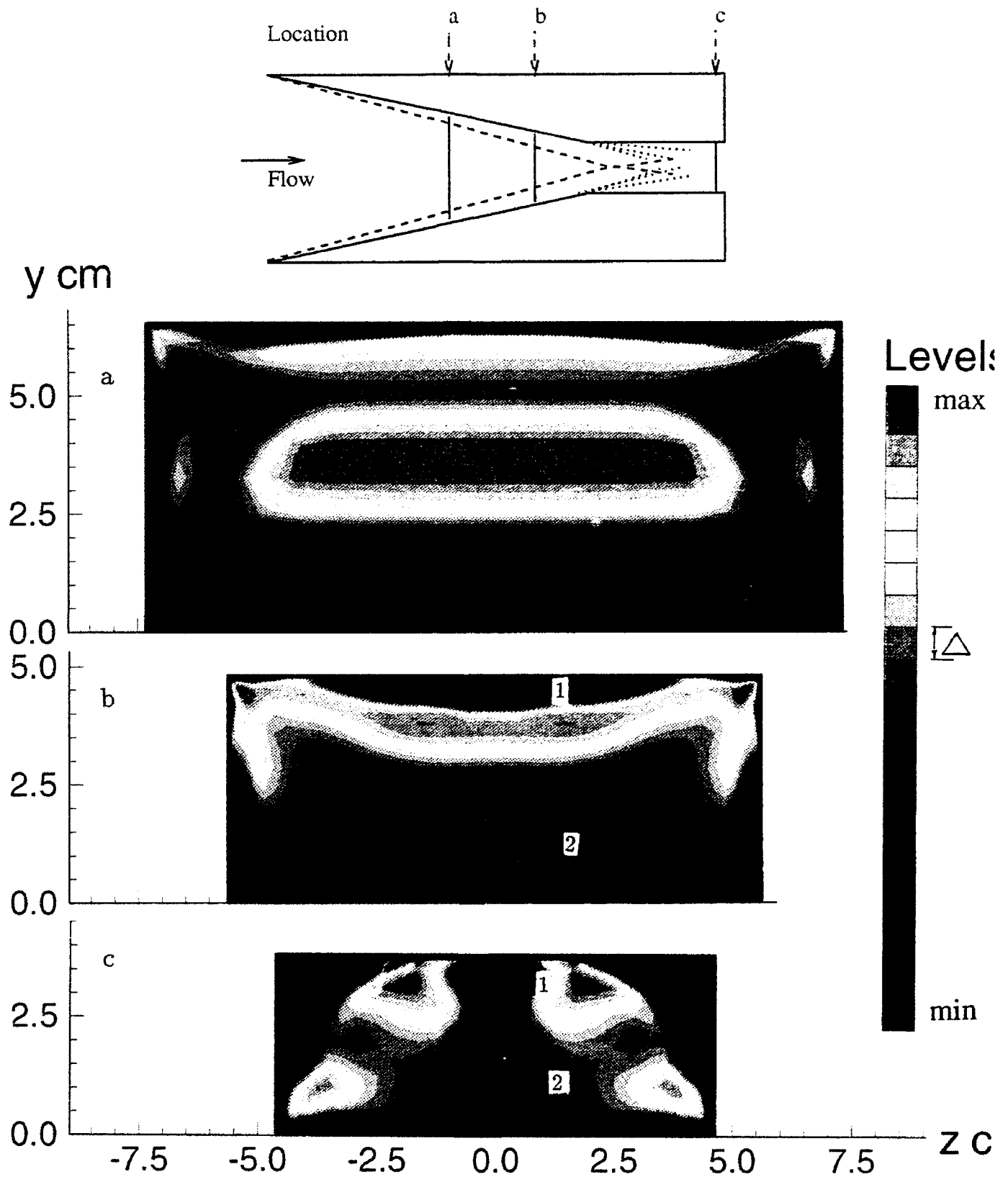


Fig.7 Computed total pressure ( $P_t/P_{t\infty}$ ) contours on cross flow planes at locations a, b and c for  $\alpha = 10^\circ$ , Mach 8.3 triple shock interaction. Contour levels : (a) min = 0.0, max = 0.94  $\Delta = 0.05$ ; (b) min = 0.0, max = 0.67,  $\Delta = 0.035$  ; (c) min = 0.0, max = 0.44,  $\Delta = 0.023$ .

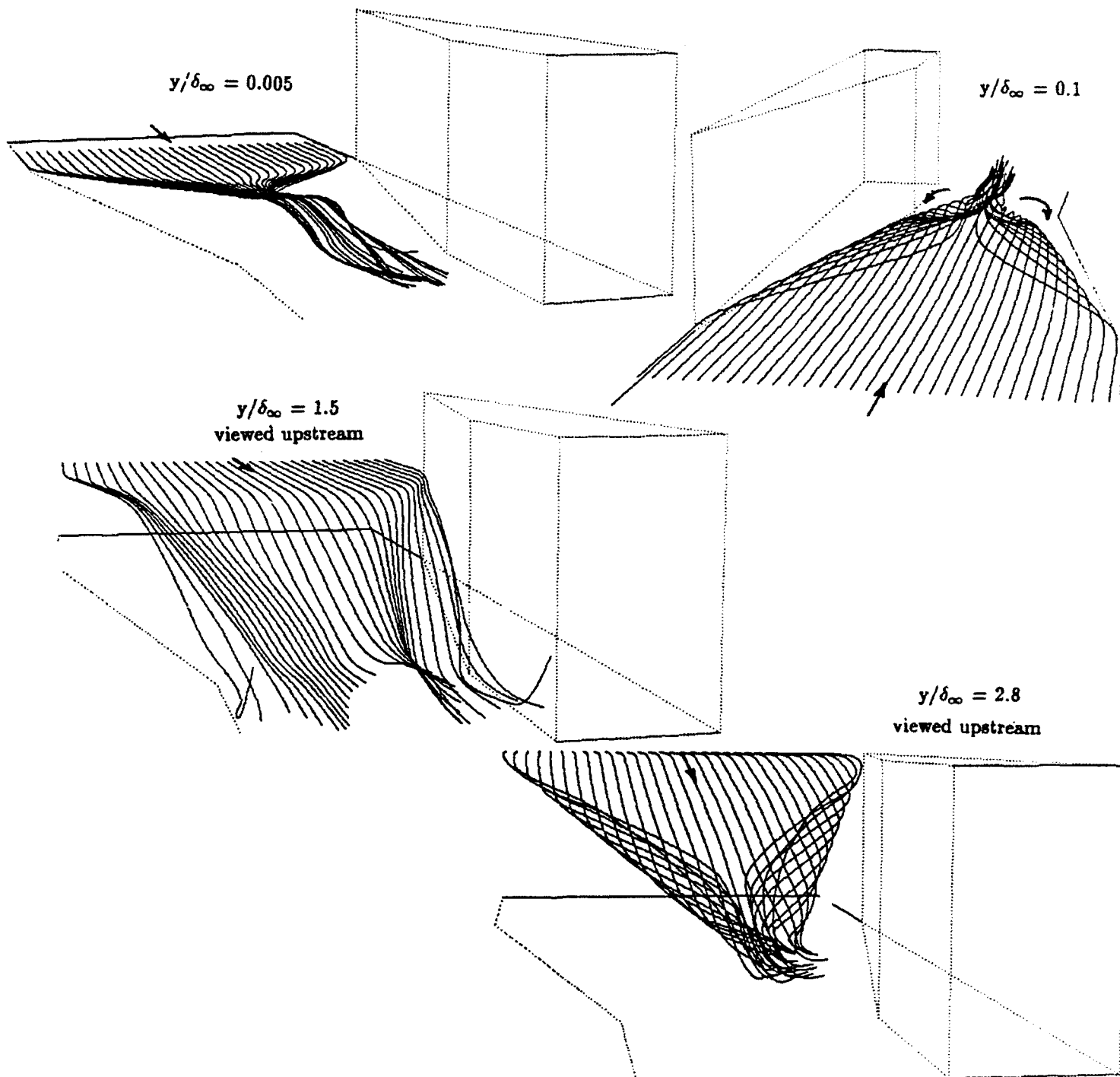


Fig.8 Computed streamline structure of  $\alpha = 10^\circ$ , Mach 8.3 triple shock interaction; particle traces originating at various  $y/\delta_\infty$  locations in upstream boundary layer

#### IV. Research program for the period : 1 October 1992 - 30 September 1993

During the period 1 October 1992 - 30 September 1993, the research program will involve two distinct (but inter-related) aspects. The first is a continued examination of complex 3-D turbulent interactions such as the crossing shock and triple shock interactions. The second is the validation of a Reynolds Stress Equation (RSE) model for compressible turbulent flows.

##### *Investigation of complex 3-D turbulent interactions*

The 3-D crossing shock interaction at supersonic Mach 4 will be examined in close collaboration with the experimental research program at the Pennsylvania State University Gas Dynamics Laboratory. The symmetric fin interaction at Mach 3.83 for  $\alpha = 15^\circ$  will be studied theoretically using the 3-D Reynolds averaged Navier-Stokes (RANS) equations in conjunction with the Baldwin-Lomax turbulence model. The computed results obtained in FY92<sup>1</sup> will be compared with the planned experimental measurements which include surface flow direction, surface pressure, skin friction, boundary layer profiles of pitot pressure and yaw angle and Planar Laser Scattering (PLS) imagery.

The asymmetric 3-D crossing shock interaction at Mach 8.3 will be examined in collaboration with the planned experiments by Drs. M. Kusoy and C. C. Horstman at the NASA-Ames Research Center. The planned experimental measurements include surface heat transfer, pressure and flow direction for at least one configuration ( $\alpha_1, \alpha_2$ ). This study represents the first collaborative theoretical / experimental effort on asymmetric crossing shock interactions.

---

<sup>1</sup>FY refers to the Federal fiscal year (i.e., October to September)

The 3-D triple shock interaction at Mach 8.3 and symmetric  $\alpha = 10^\circ$  fins has been computed using the RANS equations together with the Baldwin-Lomax turbulence model (see Section IIIC). The computed results will be compared with planned experiments by Drs M. Kussoy and C. C. Horstman at the NASA-Ames Research Center. The planned experimental measurements include surface heat transfer, pressure and flow direction, and boundary layer profiles of pitot pressure and yaw angle. This combined theoretical-experimental effort is expected to yield significant insight into the flowfield structure of the interaction.

#### *Validation of Reynolds Stress Equation model*

The Reynolds Stress Equation (RSE) turbulence model, initiated during FY92, will be evaluated for a series of compressible turbulent boundary layer flowfields. Additionally, asymptotic analysis of the constant stress layer and other simple flows will be performed to provide detailed information regarding the relationships of the model constants. The computed boundary layer results will be compared with experimental data to validate the accuracy of the RSE model. Additional effort will be focused on the development of low Reynolds number modifications to allow direct integration to solid boundaries, and other model improvements.

### V. References

- Baldwin, B. and Lomax, H., "Thin Layer Approximation and Algebraic Model for Separated Turbulent Flows", AIAA Paper No. 78-257, January 1978.
- Gaitonde, D. and Knight, D., "Numerical Experiments on the 3-D Shock Wave - Boundary layer Interaction Generated by a Sharp Fin", AIAA Paper No. 88-0309, January 1988.
- Knight, D. "A Hybrid Explicit - Implicit Numerical Algorithm for the Three-Dimensional Compressible Navier-Stokes Equations", *AIAA Journal*, Vol. 22, No. 8, August, 1984, pp. 1056-1063.

Knight, D., Horstman, C., Shapey, B. and Bogdonoff, S. "Structure of Supersonic Flow Past a Sharp Fin.", *AIAA Journal*, Vol. 25, No. 10, October 1987, pp. 1331-1337.

Knight, D. D., Horstman, C. C. and Monson, D. J., "The Hypersonic Shock Wave - Turbulent Boundary Layer Interaction Generated by a Sharp Fin at Mach 8.2", AIAA Paper No. 92-0747, January 1992.

Kussoy, M. I., Kim, K. S. and Horstman, K. C., "An Experimental Study of a Three-Dimensional Shock Wave/Turbulent Boundary Layer Interaction at a Hypersonic Mach Number," AIAA Paper No. 91-1761, June 1991.

Kussoy, M. I. and Horstman, K. C., "Intersecting Shock - Wave / Turbulent Boundary Layer Interactions at Mach 8.3", NASA TM 103909, 1992.

Narayanswami, N., Knight, D. and Horstman, C. "Investigation of a Hypersonic Shock Wave / Turbulent Boundary Layer Interaction", to appear in *Shock Waves*, November 1992.

Narayanswami, N., Knight, D., Bogdonoff S. and Horstman C. C., "The Interaction Between Crossing Oblique Shocks and a Turbulent Boundary Layer", *AIAA Journal*, Vol. 30, No. 8, August 1992, pp. 1945-1952.

Rodi, W. "Experience with Two-Layer Models Combining the  $k-\epsilon$  with a One-Equation Model Near the Wall", AIAA Paper No. 91-0216, January 1991.

Rubesin, M. and Rose, W., "The Turbulent Mean Flow Reynolds-Stress and Heat Flux Equations in Mass Averaged Dependent Variables", NASA TMX 62248, 1973.

Shang, J. S., Hankey, W. L. and Petty, J. S. "Three Dimensional Supersonic Interacting Turbulent Flow Along a Corner," *AIAA Journal*, Vol. 17, July 1979, pp. 706-713.

VanWie, D., White, M., Corpening, G., "NASP Inlet Design and Testing Issues", *Johns Hopkins APL Technical Digest*, Vol. 11, Nos. 3 and 4, 1990, pp. 353-361.

**VI. Visitors to Rutgers University : 1 March 1992 -  
30 September 1992**

Dr. C. C. Horstman (NASA-Ames Research Center)  
April 1992 (2 days),  
November 1992 (2 days).

**VII. Archival Papers : 1 March 1992 - 30 September 1992**

Knight, D., Horstman, C., and Bogdonoff, S., "The Structure of Supersonic Turbulent Flow Past a Swept Compression Corner", *AIAA Journal*, Vol. 30, April 1992, pp. 890-896.

Narayanswami, N., Knight, D., Bogdonoff, S., and Horstman, C., "The Interaction Between Crossing Oblique Shocks and a Turbulent Boundary Layer", *AIAA Journal*, Vol. 30, August 1992, pp. 1945-1952.

Knight, D., Horstman, C., Settles, G., and Zheltovodov, A., "3-D Shock Wave-Turbulent Boundary Layer Interactions Generated by a Single Fin", *The Russian Journal of Theoretical and Applied Mechanics*, Vol. 2, No. 3, June 1992.

**VIII. Videotapes: 1 March 1992 - 30 September 1992**

"Hypersonic crossing shock interaction", N. Narayanswami, C. C. Horstman and D. D. Knight, prepared by E. Pegot and V. Hirsh at the NASA-Ames Research Center

**IX. Conference papers: 1 March 1992 - 30 September 1992**

Garrison, T., Settles, G., Narayanswami, N., and Knight, D., "Structure of Crossing Shock Wave / Turbulent Boundary Layer Interactions", AIAA Paper No. 92-3670, July 1992.

Zheltovodov, A., Borisov, A., Knight, D., Horstman, C., and Settles, G., "Numerical Simulation of Shock Waves / Boundary Layer Interaction in Supersonic and Hypersonic Flows", Institute of Theoretical and Applied Mechanics, Novosibirsk, Russia, August 1992.

**X. Papers in review : 1 March 1992 - 30 September 1992**

Narayanswami, N., Horstman, C., and Knight, D., "Computation of Crossing Shock / Turbulent Boundary Layer Interaction at Mach 8.3", submitted to the *AIAA Journal*.

**XI. Presentations : 1 March 1992 - 30 September 1992**

"Shock Wave-Turbulent Boundary Layer Interactions : Status Report and Unsolved Problems", 1992 Computational Fluid Dynamics Symposium, Wright-Patterson AFB, September 1992.

"Shock Wave-Turbulent Boundary Layer Interaction", Ohio State University, September 1992.

**XII. List of personnel and degrees awarded :**  
1 March 1992 - 30 September 1992

**A. List of personnel**

*Principal Investigator :*

Prof. Doyle Knight  
Department of Mechanical and Aerospace Engineering

*Research Assistants working on this project :*

Dr. Natraj Narayanswami  
Department of Mechanical and Aerospace Engineering

Mr. Dias Badekas  
Department of Mechanical and Aerospace Engineering

**B. Degrees awarded**

Narayanswami, Natraj; Degree of Ph.D. awarded May 1992.  
Thesis: "Numerical Investigation of Crossing Shock Wave/Turbulent Boundary Layer Interactions"

**XIII. List of attached papers**

1. Narayanswami, N., Horstman, C. C., Knight, D. D., "Numerical Simulation of Crossing Shock/Turbulent Boundary Layer Interaction at Mach 8.3 - Comparison of Zero- and Two-Equation Turbulence Models, Paper No. 93-0779, AIAA 31st Aerospace Sciences Meeting, Reno, NV, January 1993.
2. Garrison, T. J., Settles, G. S., Narayanswami, N. and Knight, D., "Structure of Crossing Shock Wave / Turbulent Boundary Layer Interactions", Paper No. 92-3670, AIAA/SAE/ASME/ASEE 28th Joint Propulsion Conference, July 1992.

**Attachment No. 1**

**“Numerical Simulation of Crossing Shock/Turbulent Boundary Layer  
Interaction at Mach 8.3 - Comparison of Zero- and Two-Equation  
Turbulence Models”**

**by N. Narayanswami, C. C. Horstman and D. D. Knight**

**to be presented at the 31st Aerospace Sciences Meeting, January  
1993, Reno, NV**



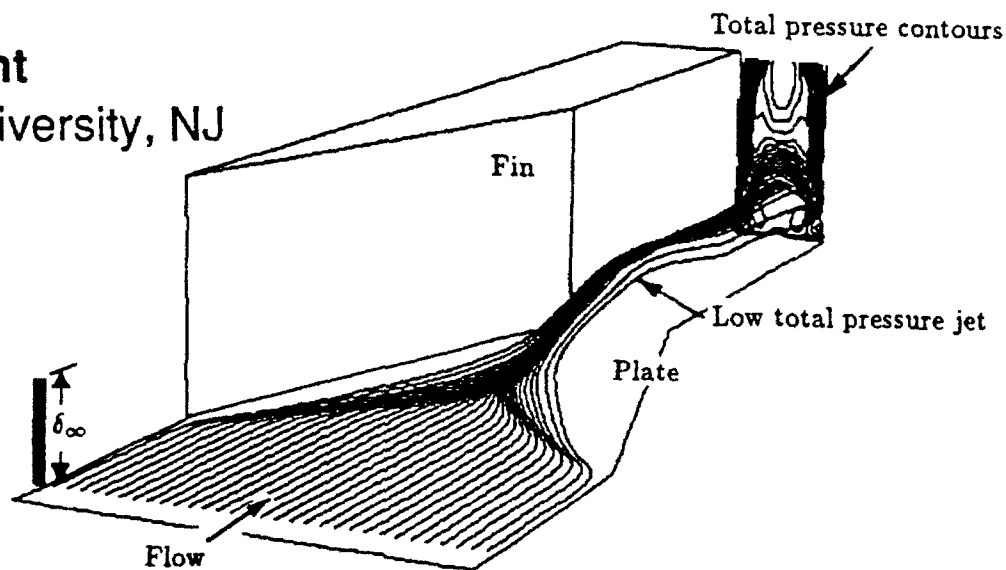
**AIAA 93-0779**

**Numerical Simulation of Crossing Shock/  
Turbulent Boundary Layer Interaction at  
Mach 8.3 - Comparison of Zero- and  
Two-Equation Turbulence Models**

**N. Narayanswami**  
Rutgers University, NJ

**C. C. Horstman**  
NASA-Ames Research Center, CA

**D. D. Knight**  
Rutgers University, NJ



Crossing shock interaction at Mach 8.3 for 15° symmetric fins: Core of low total pressure jet and total pressure distribution over the outflow boundary.

**31st Aerospace Sciences  
Meeting & Exhibit**  
January 11-14, 1993 / Reno, NV

# Numerical Simulation of Crossing Shock / Turbulent Boundary Layer Interaction at Mach 8.3

## Comparison of Zero and Two-Equation Turbulence Models

N. Narayanswami\*

*Department of Mechanical and Aerospace Engineering  
Rutgers University  
Piscataway, NJ 08855*

C. C. Horstman†

*NASA-Ames Research Center  
Moffett Field, CA 94035*

D. D. Knight‡

*Department of Mechanical and Aerospace Engineering  
Rutgers University  
Piscataway, NJ 08855*

### Abstract

A 3 - D hypersonic crossing shock wave / turbulent boundary layer interaction is examined numerically. The test geometry consists of a pair of opposing sharp fins of angle  $\alpha = 15^\circ$  mounted on a flat plate. The freestream Mach number is 8.28. Two theoretical models are evaluated. The full 3-D Reynolds-averaged Navier-Stokes (RANS) equations are solved using the Baldwin - Lomax algebraic turbulent eddy viscosity model and the Rodi (modified k- $\epsilon$ ) turbulence model. Computed results for both cases show good agreement with experiment for flat plate surface pressure and for pitot pressure and yaw angle profiles in the flowfield. General agreement is obtained for surface flow direction. Fair to poor agreement is obtained for surface heat transfer, indicating a need for more accurate turbulence models. The overall flowfield structure is similar to that observed in previous crossing shock interaction studies.

### 1. Introduction

With the resurgence of interest in high speed flight in recent years<sup>1</sup>, the problem of viscous-inviscid interaction in aerodynamic flows is once again receiving wide attention. Of particular importance is the phenomenon of three-dimensional shock wave/turbulent boundary layer interactions ("3-D turbulent interactions"). Such interactions occur in a wide variety of practical aerodynamic situations (e.g., in flows over aircraft control surfaces and within high speed inlets) and are of interest not only due to the inherent complexity and richness of the flow physics but also due to engineering challenges posed by associated problems such as large scale flow separation and increased drag and aerodynamic heating<sup>1,2</sup>.

The present study focuses on the 3 - D crossing shock interaction (Fig.1) which is typical of hypersonic inlets. The flow geometry consists of two opposing sharp fins mounted on a flat plate. The oblique shock waves, generated by the fins, intersect each other and interact with the flat plate turbulent boundary layer. Experimental investigations of crossing shock interactions include Mee *et al.*<sup>3</sup>, Batcho *et al.*<sup>4</sup>, Williams and Hingt<sup>5</sup>, Garrison and Settles<sup>6</sup>, Garrison *et al.*<sup>7</sup> and Kussoy and Horstman<sup>8</sup>. Theoretical (computational) investigations include Gaitonde and Knight<sup>9</sup>, Narayanswami *et al.*<sup>10,11</sup> and Reddy<sup>12</sup>. Computations have been performed at Mach 3 to 8.3 using the 3-D Reynolds-averaged Navier-Stokes (RANS) equations incorporating the Baldwin - Lomax turbulence model<sup>13</sup>. The computed flowfields have displayed generally good agreement with experiment for surface pressure, surface flow pattern and boundary layer profiles of pitot pressure and yaw angle. The computed heat transfer

\*Research Staff, Member AIAA

†Senior Scientist, Associate Fellow AIAA

‡Professor, Associate Fellow AIAA

has shown substantial error in comparison with experiment. With the exception of a single computation<sup>10</sup> of a crossing shock interaction at Mach 3 using the  $k-\epsilon$  model<sup>14</sup>, no turbulence model other than the Baldwin-Lomax has been examined for the crossing shock interaction.

The principal objective of the present study is to evaluate two different turbulence models, namely, (a) the Baldwin-Lomax<sup>13</sup> algebraic eddy viscosity model and (b) the Rodi (modified  $k-\epsilon$ )<sup>15</sup> model, for the crossing shock interaction in hypersonic flow. The flow at Mach 8.28 for  $\alpha = 15^\circ$  fins corresponding to the experiment of Kussoy and Horstman<sup>8</sup> is investigated. The present research effort is unique in two respects. First, it is the strongest crossing shock interaction studied to date. The overall inviscid pressure ratio (approximately 45) is substantially greater than the previous<sup>11</sup> strongest case (i.e., 19.5). Second, it is the first study to examine the relative accuracy of two different turbulence models (i.e., Baldwin-Lomax and Rodi) for hypersonic crossing shock interactions. The accuracy of the models is examined through detailed comparison with experimental data for surface pressure, surface flow pattern, surface heat transfer and flowfield surveys of pitot pressure and yaw angle. Based on the successful validation of the theoretical model(s), the flowfield structure of the interaction may be analyzed using the computed results and compared with previous studies for supersonic crossing shock interactions.

## 2. Description of experiment

The experiments were conducted in the 3.5 ft Hypersonic Wind Tunnel at the NASA-Ames Research Center<sup>3</sup>. The freestream conditions are shown in Table 1. The incoming boundary layer was fully developed and self-preserving at the fin leading edge location with a velocity profile matching the Law of Wall and Wake<sup>16</sup>. The experimental geometry is shown in Fig.1. The fin height  $H = 20$  cm ( $6.2\delta_\infty$ ) was sufficient to ensure a semi-infinite interaction. Disturbances generated by the top edges of the fins had no effect on the interaction in the region of interest, as confirmed *a posteriori* by the fin surface flow visualization results. The total fin length is  $L_e = 40.7$  cm ( $12.5\delta_\infty$ ). At a streamwise location of  $L_1 = 20.3$  cm ( $6.2\delta_\infty$ ), the fin surfaces are turned parallel to the streamwise ( $x$ ) direction. The separation distance between the fin leading edges is  $L_{sep} = 15.2$  cm ( $4.7\delta_\infty$ ).

## 3. Description of computations

The flow conditions closely match the experiment (refer Table 1). Only approximate values of the flow

conditions were known at the time of the computation, resulting in minor discrepancies between the theoretical and actual experimental values of Mach number  $M_\infty$  and total pressure  $P_{t\infty}$  (and consequently in the boundary layer thickness parameters and Reynolds number  $Re_{\delta_\infty}$ ).

The governing equations are the 3-D Reynolds-averaged Navier-Stokes equations using mass averaged variables<sup>17</sup> in strong conservation form<sup>18</sup>. The Baldwin-Lomax and the Rodi (modified  $k-\epsilon$ ) turbulence models were employed. The molecular dynamic viscosity was specified by Sutherland's law<sup>19</sup>. The molecular Prandtl number is 0.73 (air) and the turbulent Prandtl number is 0.9. The perfect gas equation of state was employed, since real gas effects are negligible under the present flow conditions<sup>20</sup>.

For simplicity, the fin boundary layer was assumed to be turbulent from the leading edge. Although this assumption differs from the experiment, in which the fin boundary layer (in the region outside of the plate boundary layer) transitions to turbulent at approximately 21 cm downstream of the fin leading edge (determined empirically using the method of Deem and Murphy<sup>21</sup>), the effect of the modification is limited to the fin boundary layer. The flowfield in the region of interest is unaffected. Results of previous computations by Knight *et al.*<sup>22</sup> for the 3-D single fin interaction at Mach 8.2 and by Narayanswami *et al.*<sup>11</sup> for the  $\alpha = 10^\circ$  crossing shock interaction at Mach 8.3 support the above statement.

The symmetry of the experimental geometry along the central  $x$ - $y$  plane permits reduction of the actual computational domain to one-half of the experimental domain. On the inflow boundary, the 2-D turbulent boundary layer profile matching the experiment was prescribed. On the plate and fin surfaces, the velocity vector, turbulent kinetic energy ( $k$ ), rate of dissipation of turbulent kinetic energy ( $\epsilon$ ) and the normal gradient of static pressure were set to zero. The temperature was set to the experimental value. On the symmetry boundaries (upstream of the fin leading edge and the centerplane), the normal component of velocity and the normal derivatives of the remaining velocity components, static pressure, temperature and  $k$  and  $\epsilon$  were set to zero. A zero gradient condition was employed at the top and outflow boundaries. The Baldwin-Lomax computation employed the hybrid explicit-implicit scheme of Knight<sup>23</sup>. The Rodi computation employed the hybrid scheme of MacCormack<sup>24</sup>.

The computational domain is shown in Fig.1b. In the experiment, the fins are terminated at a distance  $L_e = 40.7$  cm. In the computations, the body-fitted grid near the trailing edges is simplified by including a diverging duct of angle  $\theta = 20^\circ$  and  $10^\circ$  for the

Baldwin - Lomax and Rodi computations, respectively. The streamwise length of the computational domain was thus extended up to  $L_c = 50.7$  cm ( $15.6\delta_\infty$ ) for the Baldwin - Lomax case and  $55.55$  cm ( $17.1\delta_\infty$ ) for Rodi case. The inclusion of the duct does not affect the flowfield in the region surrounding the crossing shocks. This is supported by the *a posteriori* observation that the computed flowfield at  $x = L_c$  is supersonic everywhere except extremely close to the plate and fin surfaces.

The grid spacings adequately resolve the flowfield and meet all the criteria for grid resolution employed in previous 3-D turbulent interaction studies<sup>7,10,11,25</sup>. Details of the grids are provided in Table 2. The total number of grid points and degree of resolution in the two computations are similar. The inflow boundary is in a region of undisturbed flow. Non-uniform spacing is employed in all three directions. The minimum  $x$  grid spacing ( $0.15\delta_\infty$ ) is in the region surrounding the crossing shocks. In the cross flow ( $y-z$ ) plane, the grids in the two directions are generated using simple geometric stretching with minimum spacings adjacent to the solid surfaces. In the Baldwin - Lomax computation, the first point adjacent to the plate satisfies  $y^+ \leq 0.63$  at all locations, where  $y^+ = yu^*/\nu_w$  and  $u^* = \sqrt{\tau_w/\rho_w}$  is the local friction velocity,  $\tau_w =$  wall shear stress,  $\rho_w =$  density at the wall and  $\nu_w =$  kinematic viscosity at the wall. The average value of  $y^+$  is 0.18. The first point off the fin surface satisfies  $z^+ \leq 1.97$ , the average value being 0.67. In the Rodi computation, the first point off the flat plate and fin surfaces satisfies  $y^+ \leq 1.0$  and  $z^+ \leq 1.0$ , the average values being 0.4 and 0.3, respectively. The plate and fin boundary layers contain typically 30 and 20 grid points, respectively, in both computations. The maximum spacing in the  $y$  direction (in the freestream) is  $0.16\delta_\infty$  for the Baldwin - Lomax case and  $0.14\delta_\infty$  for the Rodi case. The spacing in the  $z$  direction in the freestream varies along the streamwise ( $x$ ) direction, due to narrowing of the physical domain. The maximum  $z$ -grid spacing is  $0.22\delta_\infty$  for the Baldwin - Lomax computation and  $0.1\delta_\infty$  for the Rodi computation, at the upstream boundary.

The initial condition in both computations was obtained by propagating the 2-D inflow boundary layer profile to all downstream locations. Convergence was determined by monitoring changes in specific flow variables (density, streamwise velocity and total energy) over characteristic time spans  $T_c (= L/U_\infty)$ . At convergence, the relative change in the above flow variables over  $1 T_c$  was typically less than 0.1% at all locations. The computations each required a total integration time of approximately 4 - 5  $T_c$  for convergence.

## 4. Comparison with experiment

### 4.1 Surface pressure

Comparison between the computed and experimental surface pressure distribution shows good agreement. Experimental flat plate surface pressure measurements were taken along the interaction centerline and along transverse cuts at various streamwise locations (refer Fig.2). The computed and experimental results along the centerline are shown in Fig.3. The general shape of the distribution, extent of upstream influence, and the locations of the first maximum (at  $x/\delta_\infty = 6.8$ ) and minimum (at  $x/\delta_\infty = 9.0$ ) are predicted reasonably well by both computations. The peaking of the pressure is a result of the intersection of the primary shocks (see "I1" in Fig.1b). The subsequent drop in pressure results from the expansion fan originating at the turn in the fin geometry at  $x/\delta_\infty = 6.26$  (see "E" in Fig.1b). The magnitude of the peak pressure is over-predicted in both cases by approximately 20%. The observed peak pressure is nearly one half of the inviscid value, indicating significant combined influence of viscous effects and the expansion fan. A second (smaller) peak is observed further downstream at approximately  $x/\delta_\infty = 10.0$  and is associated with the second crossing of the reflected shocks (see "I2" in Fig.1b). The magnitude of this second peak and the general distribution of pressure downstream of  $x/\delta_\infty = 9.5$  are predicted accurately by the Baldwin - Lomax computation but are overestimated in the Rodi case. Examination of the experimental fin surface streamlines (not shown) indicates significant streamwise separation at approximately  $x/\delta_\infty = 6.5$ . Similar results are observed for the Baldwin - Lomax computation. The Rodi computation, however, does not show any such streamwise separation. Consequently, in the Rodi case, the shocks reflecting off the fin surfaces are stronger than in the Baldwin - Lomax case, and lead to higher pressures downstream of their intersection.

Comparison between computation and experiment for the various transverse cuts shows similar results (Fig.4). The locations a, b and c correspond to  $x/\delta_\infty = 5.6, 6.92$  and  $8.31$ , respectively (refer Fig.2). At location a, the Rodi computation predicts the pressure distribution more accurately than the Baldwin - Lomax computation. The experimental pressure near the centerline exceeds the inviscid level due to the upstream influence of the interaction. Away from the centerline, the pressure level falls below the local inviscid level due to the reflection of the expansion fan (which is part of the " $\lambda$ " structure of the initial single fin interaction - discussed in Sec. 5.2) off the fin surface. At locations b and c, the two computations display

reasonable agreement with experiment. At location b, just downstream of the crossed shocks, the maximum pressure is at the centerline due to the formation of a localized shock structure in that region (Sec. 5.2). The steep fall in pressure away from the centerline is caused by the expansion fan originating from a turn in the fin geometry at  $x/\delta_\infty = 6.26$ . At location c, further downstream, the influence of the expansion fan is stronger and the maximum pressures are near the fin surfaces with the lowest pressure occurring near the centerline.

#### 4.2 Pitot pressure

The experimental and computed results for pitot pressure ( $P_p/P_{p\infty}$ ) are shown in Figs.5(a-f). The results are displayed as color contours on cross flow ( $y-z$ ) planes (locations shown in Fig.2). Note that a separate color scale is used for each plane. Locations (a,b), (c,d) and (e,f) correspond to  $x/\delta_\infty = 5.6, 6.92$  and  $8.31$ , respectively. The experimental measurements do not extend fully to the fin and plate surfaces. The region of computation is truncated to match the region of experimental measurement.

There is overall good agreement between the experiment and both computations. At  $x/\delta_\infty = 5.6$  (Figs.5a, b), a large low pitot pressure region (marked "1") is observed in the region  $y/\delta_\infty < 0.8$ . This structure<sup>10,11</sup> is associated with a low total pressure jet comprising two helical counter-rotating vortices (see Sec. 5.1), and is evident at subsequent stations (Figs.5c-f). The sharp change of contour levels in the region  $0.1 \leq z/\delta_\infty \leq 0.2, y/\delta_\infty > 1.0$  indicates the primary shock. The shape and extent of the low pitot pressure region are predicted fairly accurately by both computations. At  $x/\delta_\infty = 6.92$  and  $8.31$  (Figs.5(c-f)), there is general qualitative agreement between the computations and experiment, with the Rodi computation displaying overall better accuracy than the Baldwin - Lomax computation. In both cases, the computed low pitot pressure region is somewhat flattened, compared to the experiment.

#### 4.3 Yaw angle

The results for computed and experimental yaw angle profiles in the flowfield are shown in Fig.6. The yaw angle is defined by  $\tan^{-1}(w/u)$  where  $w$  is the cross-flow velocity (in the  $z$  direction) and  $u$  is the streamwise velocity (in the  $x$  direction), and represents the local direction of the velocity vector in a plane parallel to the flat plate. Experimental yaw angle surveys were conducted at  $x/\delta_\infty = 5.6, 6.92$  and  $8.31$ , similar to the pitot pressure surveys. At  $x/\delta_\infty = 5.6$ , the locations a

through d denote distances away from the centerline of  $z/\delta_\infty = -0.65, -0.49, -0.33$  and  $-0.16$ , respectively (i.e., the survey stations are to the left of the centerline). At locations  $x/\delta_\infty = 6.92$ , and  $x/\delta_\infty = 8.31$ , the locations a through c denote distances away from the centerline of  $z/\delta_\infty = -0.48, -0.32$  and  $-0.15$ , respectively.

There is overall general agreement between the computed and experimental results. At  $x/\delta_\infty = 5.6$ , there is close agreement between computation and experiment. The large yaw angles near the plate (up to approximately  $y/\delta_\infty = 0.5$ ) indicate the turning of streamlines under the low total pressure jet (Sec. 4.2), towards the centerline. These streamlines originate close to the edge of the boundary layer in the upstream (incoming) flow. The wrapping of these streamlines under the rising low total pressure jet is particularly evident from the profile at location d (closest to the centerline) as seen from the increase in yaw angle from zero (at the wall) to approximately  $30^\circ$  at base of the jet. At  $x/\delta_\infty = 6.92$ , the comparison between computation and experiment is generally good. At locations a and b, the flow is between the bulk of the low total pressure jet (refer Figs.5c,d) and the fin surface. The flow direction is hence generally parallel to the fin walls (yaw angles close to zero). At location c, the profile is through the core of the low total pressure jet. The relatively large yaw angles (approximately  $11^\circ$ ) in the region  $y/\delta_\infty \leq 0.1$  indicate the sweeping of streamlines at the base of the jet, towards the centerline. Away from the plate, the decrease of the yaw angle to values less than zero is associated with the anti-clockwise rotation of the vortex (which is part of the jet) to the left of the centerline. The subsequent increase in yaw angle to positive values, with a maximum at approximately  $y/\delta_\infty = 0.8$  is associated with the streamlines originating at  $y/\delta_\infty > 1.0$  in the upstream boundary layer. Further away from the plate, the yaw angle is close to zero due to the turning of streamlines in the freestream parallel to the local direction of the fin surface, by the reflected shocks. At  $x/\delta_\infty = 8.31$ , the computed profiles show increasing differences with experiment at larger distances from the centerline. The flow physics near the fin surface is further complicated by the influence of the expansion fan originating at the fin surface at  $x/\delta_\infty = 6.26$ . The profiles through the low total pressure jet (at locations b and c) are qualitatively similar to that at  $x/\delta_\infty = 6.92$ .

Overall, there is very close agreement between the two computations at all locations. This result is surprising, since comparison of the computed eddy viscosity values in the two cases (Fig.7) at the above locations display differences in the peak values by as much as a factor of 7. It is thus inferred that the flowfield is primarily rotational and inviscid, with viscous and

turbulence effects restricted to a thin layer adjacent to the solid surfaces.

#### 4.4 Surface flow pattern

The computed and experimental surface flow patterns show general overall agreement (Figs.8a-c). In the upstream portion of the interaction ( $x/\delta_\infty < 3.0$ ), the flow pattern on either side of the centerline is initially similar to that for single fin interactions<sup>25</sup>. Key features, such as the lines of the lines of coalescence (LC) and the lines of divergence (LD) are observed clearly in the experiment and in both computations. The strong lines of coalescence are clear indicators of large scale flow separation (in the sense of Lighthill<sup>26</sup>) and evidence for this phenomenon is presented in a discussion of the overall streamline structure of the interaction in Sec. 5.1.

The computational results show additional unusual features. In the Baldwin - Lomax case (Fig.8b), the two lines of coalescence appear to converge onto a node at the centerline. A saddle point (from which all streamlines diverge) is observed downstream of the node. In the region between the node and saddle point, the general flow direction is upstream (i.e., in the reverse streamwise direction), indicating the existence of a local separation bubble (in the 2-D sense). This feature is clearly absent in the Rodi case (Fig.8c). The experimental results are unclear in this region, leaving the accuracy of computed results open to question. Downstream of the local separation zone (between  $x/\delta_\infty = 3.07$  and 6.15), the Baldwin - Lomax results show a converging - diverging - re-converging "coke-bottle" pattern near the centerline, the envelope of the streamlines formed by local lines of coalescence. The flow within the diverging segment is turned away from the centerline. A similar pattern is observed in the Rodi case, the diverging segment forming somewhat earlier (more upstream) than in the Baldwin-Lomax case. In the downstream portion of the interaction ( $x/\delta_\infty > 6.15$ ), the two computations show close agreement with experiment. The flow physics in this region is complex and the correspondence between the features observed in the surface flow pattern and the flow structures away from the plate (such as the low total pressure jet, corner vortices and shocks/expansions) is as yet not fully understood.

#### 4.5 Surface heat transfer

The computed and experimental surface heat transfer distributions show overall fair to poor agreement. Experimental flat plate heat transfer measurements were taken along the interaction centerline and along

transverse cuts at the streamwise locations of  $x/\delta_\infty = 5.08, 6.4,$  and  $7.78$  (refer Fig.2). The computed and experimental results along the centerline are shown in Fig.9. Both computations show good qualitative agreement with experiment with regard to the general shape of the profile. The initial drop in heat transfer in the region  $1.0 \leq x/\delta_\infty \leq 3.0$  is predicted more accurately by the Baldwin - Lomax computation. However, there is significant disagreement between both computations and experiment in the region  $3.0 \leq x/\delta_\infty \leq 5.0$ , the Baldwin - Lomax computation underestimating the heat transfer by as much as 90%. Beyond  $x/\delta_\infty = 5.0$ , the Baldwin - Lomax computation shows better overall agreement with the experimental data than the Rodi computation. The peak heat transfer is overpredicted by both computations by approximately 20%.

The comparison between computation and experiment along transverse cuts (Fig.10a-c) shows poor agreement. Both computations generally overpredict the experimental values. At  $x/\delta_\infty = 6.4$  and  $7.78$  (locations b and c), the peak heat transfer is overestimated by the Baldwin - Lomax computation by approximately 50% and 75%, respectively. The overestimation in the Rodi case is comparable. The sharply peaked distributions in the case of the Baldwin - Lomax computation is due to sharp changes in the magnitude of the local length scale computed by the turbulence model.

### 5. Flowfield structure

Notwithstanding the discrepancy between the computed and experimental values of surface heat transfer, the prediction of the flowfield (at least away from the solid surfaces) is fairly accurate in both computations, as evidenced by the overall good agreement between the computations and experiment for surface pressure and pitot pressure and yaw angle profiles. The computed results are thus analyzed to determine the flowfield structure of the interaction.

#### 5.1 Streamline structure

The streamline structure of the interaction determined from both the Baldwin - Lomax and Rodi computations show close agreement. The structure is similar to that observed in previous studies of crossing shock interactions<sup>7,10,11</sup>. The principal feature of the streamline structure is a low total pressure jet comprising two weakly counter rotating vortices whose cores are formed by streamlines originating from close to the flat plate within the incoming boundary layer. The trajectories of particles originating at  $y/\delta_\infty = 0.005$

(Fig.11a) show the core flow. The two counter-rotating vortices are initially formed due to the individual single fin interactions<sup>25</sup> in the upstream portion of the flow, as indicated by the trajectories of particles originating at  $y/\delta_\infty = 0.25$  (Fig.11b). The two vortices "collide" at the centerline and lifted away from the flat plate in the form of a jet. This jet structure is also evident from the low pitot pressure contours observed in Figs.5(a-f). Streamlines originating from higher up within the boundary layer (e.g. at  $y/\delta_\infty = 0.75$ , Fig.11c) wrap around and underneath the lifting low total pressure jet (note the relatively higher pitot pressures away from the centerline at the base of the low pitot pressure regions in Figs.5(a-f)). Streamlines originating close to the edge of the boundary layer (e.g. at  $y/\delta_\infty = 1.0$ , Fig.11d) are deflected by the local "inviscid" portions of the primary and reflected shocks and continue streamwise over the low total pressure jet underneath.

## 5.2 Wave structure

The wave structure of the interaction is similar to that observed in previous studies of crossing shock interactions<sup>7,10,11</sup>. Figs.12(a-d) show contours of static pressure ( $P/P_\infty$ ) on cross-flow ( $y-z$ ) planes at  $x/\delta_\infty = 2.15, 3.57, 5.23$  and  $7.38$ , respectively. The color bar indicates the range of  $P/P_\infty$  on the particular cross-flow plane. A schematic of the shock waves and expansion fans determined from the static pressure contours at each location, is shown alongside.

The two computations show close agreement. The comparison is shown by presenting the results of the two cases as the two halves of the cross-flow plane. At location a, ( $x/\delta_\infty = 2.15$ ), the "λ" shaped shock structures of the individual single fin interactions are evident. The primary shock (1) bifurcates<sup>27</sup> into a separation shock (2) and a rear shock (3). A slip line (not shown) emanates from the triple point (intersection of shocks 1,2 and 3) and curves into the fin-plate junction. The separation vortex is aligned approximately with the primary shock, at the base of the shock. The flow between the vortex and slip line is turned by an expansion fan (not shown). At location b ( $x/\delta_\infty = 3.57$ ), a conical<sup>7</sup> "∩" shaped reflected shock (4a,b) has developed due to the interaction of the two separation shocks. This conical shock grows outward, away from the centerline. At location c ( $x/\delta_\infty = 5.23$ ), the interaction of the curved portion of the conical shock (4b) with the rear shock (3) has resulted in a region of local high pressure (6). The central segment of the conical shock (4a) remains unaffected. A new shock structure (5) is observed near the flat plate over the interaction centerline. At location d ( $x/\delta_\infty = 7.38$ ), the

primary shocks have crossed and the reflected shocks (7) are clearly evident. Shock 4a appears to continue upward, between the two reflected shocks. An expansion fan (8) is formed between the reflected shocks, below shock 4a. This expansion fan is the mechanism for the turning of the low total pressure jet parallel to the flat plate, downstream of the crossed shocks (refer Sec. 5.1). The shock over the centerline (5) is still present.

There are, however, some differences between the wave structure described above and that determined experimentally<sup>6,7</sup> at Mach 4. In the present case, only the central portion (4a) of the conical shock remains after interaction with the rear shock (3). The Mach 4 experimental results, however, indicate that the entire conical shock (including the curved portion (4b)) continues to grow outward after interaction with the rear shock. This difference is perhaps due to the fact that the expansion fans originating from the fin surface at  $x/\delta_\infty = 6.26$  in the present case interact with and significantly weaken the curved portions of the conical shock. No such expansion fans were present in the Mach 4 case. There is a clear need for direct experimental flowfield visualization of the present case to resolve the above issues.

## 6. Conclusions

The 3-D crossing shock interaction at Mach 8.3 for symmetric 15° fins was investigated theoretically (numerically) using the RANS equations and two turbulence models. The following conclusions have been reached :

- Computed results for surface pressure and profiles of pitot pressure and yaw angle for both the Baldwin - Lomax and Rodi models are similar and show generally good agreement with experiment. Neither model accurately predicts surface heat transfer indicating a need for more accurate turbulence models.
- The streamline and wave structures of both models are in good agreement and similar to the results at lower (supersonic) Mach numbers. The principal feature of the streamline structure is the formation of a low total pressure jet comprising two weakly counter-rotating vortices.
- The close agreement between the two computations with regard to the mean velocity field, despite considerable differences in the computed eddy viscosity distribution, indicates that the flowfield is primarily rotational and inviscid, with viscous and turbulence effects being limited to a thin layer adjacent to solid surfaces.

## Acknowledgments

This research was sponsored by the AFOSR under Grant No. 86-0266 monitored by Dr. L. Sakell and by NASA-Ames Research Center. Supercomputer resources were provided by the National Center for Supercomputing Applications (NCSA) by Cray Research Inc. through the University Research and Development Grant program and by the NASA-Ames Research Center. Analysis of the computed results was performed at the Rutgers University- Supercomputer Remote Access Facility.

## References

- <sup>1</sup>VanWie, D., White, M., Corpening, G., "NASP Inlet Design and Testing Issues", *Johns Hopkins APL Technical Digest*, Vol. 11, Nos. 3 and 4, 1990, pp. 353-361.
- <sup>2</sup>Settles, G. and Dolling, D., "Swept Shock / Boundary Layer Interactions - Tutorial and Update", AIAA Paper No. 90-0375, January 1990.
- <sup>3</sup>Mee, D., Stalker, R., Stollery, J., "Glancing Interactions Between Single and Intersecting Oblique Shock Waves and a Turbulent Boundary Layer", *Journal of Fluid Mechanics*, Vol. 170, 1986, pp. 411-433.
- <sup>4</sup>Batcho, P. F., Ketchum, A. C., Bogdonoff, S. M. and Fernando, M., "Preliminary Investigation of the Interactions Caused by Crossing Shock Waves and a Turbulent Boundary Layer", AIAA Paper No. 89-0359, January 1989.
- <sup>5</sup>Williams, K. E., and Hingst, W. R., "The Effect of Varying Mach Number on Crossing, Glancing Shocks / Turbulent Boundary Layer Interactions", AIAA Paper No. 91-2157, June 1991.
- <sup>6</sup>Garrison T. J. and Settles, G. S., "Flowfield Visualization of Crossing Shock-Wave / Boundary Layer Interactions", AIAA Paper No. 92-0750, January 1992.
- <sup>7</sup>Garrison, T. J., Settles, G. S., Narayanswami, N., and Knight, D., "Structure of Crossing Shock Wave / Turbulent Boundary Layer Interactions", AIAA Paper No. 92-3670, July 1992.
- <sup>8</sup>Kussoy, M. I. and Horstman, K. C., "Intersecting Shock - Wave / Turbulent Boundary Layer Interactions at Mach 8.3", NASA TM 103909, 1992.
- <sup>9</sup>Gaitonde, D. and Knight, D., "Numerical Experiments on the 3-D Shock Wave - Boundary layer Interaction Generated by a Sharp Fin", AIAA Paper No. 88-0309, January 1988.
- <sup>10</sup>Narayanswami, N., Knight, D., Bogdonoff S. and Horstman C. C., "The Interaction Between Crossing Oblique Shocks and a Turbulent Boundary Layer", *AIAA Journal*, Vol. 30, No. 8, August 1992, pp. 1945-1952.
- <sup>11</sup>Narayanswami, N., Knight, D. and Horstman, C., "Investigation of a Hypersonic Shock Wave / Turbulent Boundary Layer Interaction", to appear in *Shock Waves*, November 1992.
- <sup>12</sup>Reddy, D. R., "3-D Navier-Stokes Analysis of Crossing, Glancing Shocks / Turbulent Boundary Layer Interactions", AIAA Paper No. 91-1758, June 1991.
- <sup>13</sup>Baldwin, B. and Lomax, H. "Thin Layer Approximation and Algebraic Model for Separated Turbulent Flows", AIAA Paper No. 78-257, January 1978.
- <sup>14</sup>Jones, W. and Launder, B., "The Prediction of Laminarization with a Two-Equation Model of Turbulence", *Int. Journal of Heat and Mass Transfer*, Vol. 15, 1972, pp. 301-304.
- <sup>15</sup>Rodi, W., "Experience with Two-Layer Models Combining the  $k-\epsilon$  with a One-Equation Model Near the Wall", AIAA Paper No. 91-0216, January 1991.
- <sup>16</sup>Sun, C. C. and Childs, M. E., "A Modified Wall Wake Velocity Profile for Turbulent Compressible Boundary Layers", *Journal of Aircraft*, Vol. 10, No. 6, June 1973, pp. 381-383.
- <sup>17</sup>Rubesin, M. and Rose, W., "The Turbulent Mean Flow Reynolds-Stress and Heat Flux Equations in Mass Averaged Dependent Variables", NASA TMX 62248, March 1973.
- <sup>18</sup>Pulliam, T. and Steger, J., "Implicit Finite-Difference Simulations of Three-Dimensional Compressible Flow", *AIAA Journal*, Vol. 18, pp. 159-167.
- <sup>19</sup>Ames Research Staff, "Equations, Tables and Charts for Compressible Flow", NACA Report 1135, 1953, p.19.
- <sup>20</sup>Anderson, J. D., *Hypersonic and High Temperature Gas Dynamics*, McGraw Hill, New York.
- <sup>21</sup>Hopkins, E., Jillie, O. and Sorensen, V. "Charts for Estimating Boundary-Layer Transition on Flat Plates", NASA TN D-5846, 1970.

<sup>22</sup>Knight, D. D., Horstman, C. C. and Monson, D. J., "The Hypersonic Shock Wave - Turbulent Boundary Layer Interaction Generated by a Sharp Fin at Mach 8.2", AIAA Paper No. 92-0747, January 1992.

<sup>23</sup>Knight, D., "A Hybrid Explicit - Implicit Numerical Algorithm for the Three-Dimensional Compressible Navier-Stokes Equations", *AIAA Journal*, Vol. 22, No. 8, August 1984, pp. 1056-1063.

<sup>24</sup>MacCormack, R. W., "A Numerical Method for Solving the Equations of Compressible Viscous Flow", *AIAA Journal*, Vol. 20, No. 9, September 1982, pp. 1275-1281.

<sup>25</sup>Knight, D., Horstman, C., Shapey, B. and Bogdonoff, S., "Structure of Supersonic Flow Past a Sharp Fin.", *AIAA Journal*, Vol. 25, No. 10, October 1987, pp. 1331-1337.

<sup>26</sup>Lighthill, M., "Introduction to Boundary Layer Theory", *Laminar Boundary Layer*, ed. Rosenhead, L., Oxford University Press, 1963, pp. 72-82.

<sup>27</sup>Alvi, F. S. and Settles, G. S., "Structure of Swept Shock Wave/Boundary Layer Interactions Using Conical Shadowgraphy", AIAA Paper No. 90-1644, June 1990.

Table 1 Flow Conditions<sup>a</sup>

	$\delta_\infty$ (cm)	$\delta_\infty^*$ (cm)	$M_\infty$	$Re_{\delta_\infty}$	$P_{t\infty}$ (kPa)	$T_{t\infty}$ (K)	$T_w$ (K)
Experiment	3.25	1.26	8.28	$1.7 \times 10^5$	5220	1111	300
Baldwin-Lomax	3.0	1.38	8.20	$1.6 \times 10^5$	4900	1111	300
Rodi	3.0	1.22	8.18	$1.6 \times 10^5$	4822	1111	300

<sup>a</sup>Legend:  $\delta$  = boundary layer thickness,  $\delta^*$  = displacement thickness,  $M$  = Mach number,  $Re$  = Reynolds number,  $P_t$  = total pressure,  $T_t$  = total temperature,  $T_w$  = wall temperature (fin and plate surfaces), subscripts:  $\infty$  = evaluated in freestream,  $\delta$  = evaluated based upon boundary layer thickness

Table 2 Grid Details<sup>a</sup>

x - direction					
	$N_x$	$\Delta x / \delta_\infty^\dagger$	$x_{inflow} / \delta_\infty$	$x_{outflow} / \delta_\infty$	
Baldwin-Lomax	100	0.15	-4.63	15.6	
Rodi	100	0.15	-1.26	17.1	
y - direction					
	$N_y$	$\Delta y / \delta_\infty  _{min}$	$\Delta y / \delta_\infty  _{max}$	$y_{max} / \delta_\infty$	
Baldwin-Lomax	72	$0.56 \times 10^{-4}$	0.16	7.39	
Rodi	64	$0.25 \times 10^{-4}$	0.14	6.0	
z - direction					
	$N_z$	$\Delta z / \delta_\infty  _{min}$	$\Delta z / \delta_\infty  _{max}$	$z_{max} / \delta_\infty$	
Baldwin-Lomax	35	$1.81 \times 10^{-4}$	0.22	2.34	
Rodi	40	$0.25 \times 10^{-4}$	0.1	2.34	
	$\Delta y^+  _{plate}$		$N_{plate}$	$\Delta z^+  _{fin}$	
	avg	max		avg	max
Baldwin-Lomax	0.18	0.63	30	0.67	1.97
Rodi	0.4	1.0	30	0.3	1.0

<sup>a</sup>Legend:  $\delta$  = boundary layer thickness,  $N_x, N_y, N_z$  = number of points along x, y and z directions, respectively,  $\Delta x, \Delta y, \Delta z$  = grid spacings in the x, y and z directions, respectively,  $\Delta y^+ |_{plate}, \Delta z^+ |_{fin}$  = distance of first point adjacent to flat plate and fin surfaces, respectively,  $N_{plate}, N_{fin}$  = typical number of points in the boundary layer on flat plate fin surfaces, respectively, subscripts: *in, out* = at inflow, outflow planes, *max* = maximum, *min* = minimum,  $\infty$  = evaluated in freestream, superscripts:  $\dagger$  implies variable grid spacing; reported values are in vicinity of inviscid shock intersection, + implies wall units, i.e., distances are normalized by the local viscous length scale  $\nu_w / u_w$ .

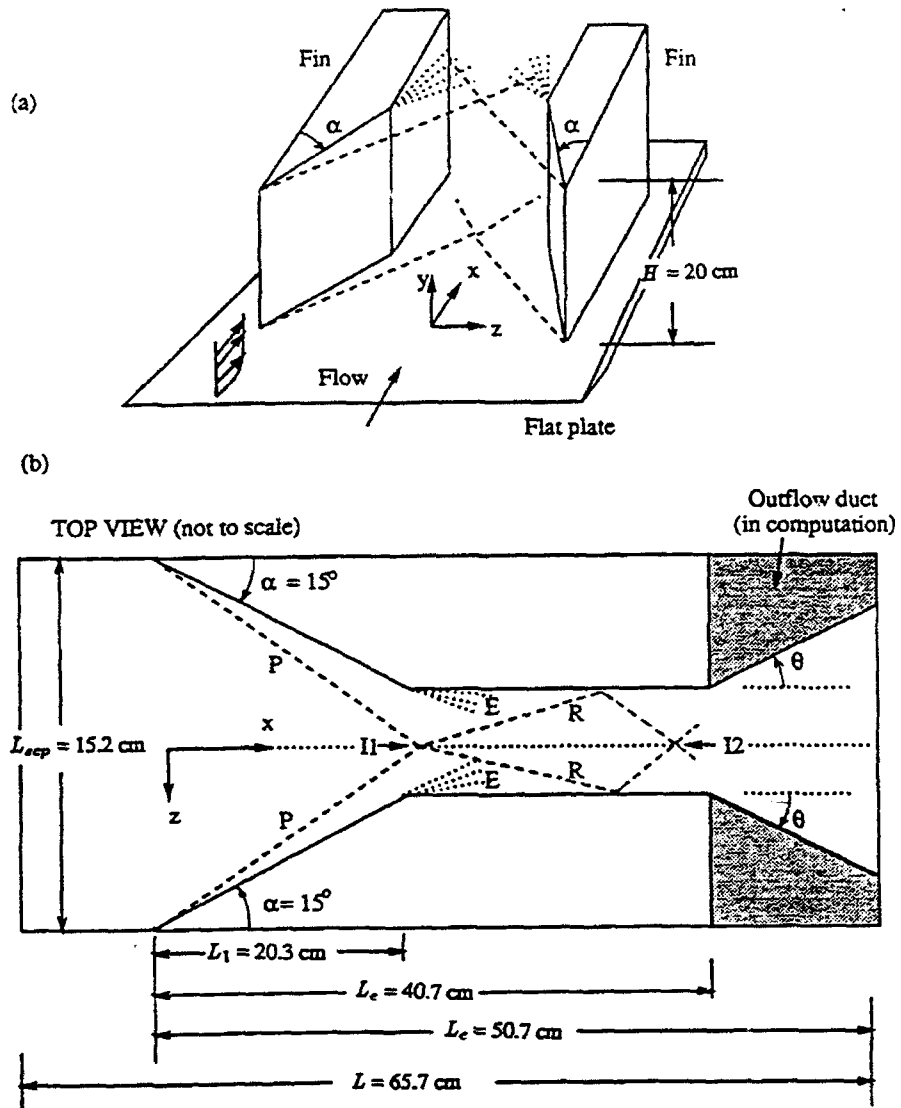


Fig.1 Crossing shock interaction : (a) experimental domain, (b) computational domain, Legend :  $\alpha$  = fin angle,  $\theta$  = outflow duct angle, P = primary shock, E = expansion fan, R = reflected shock, I1, I2 = inviscid shock intersection locations.

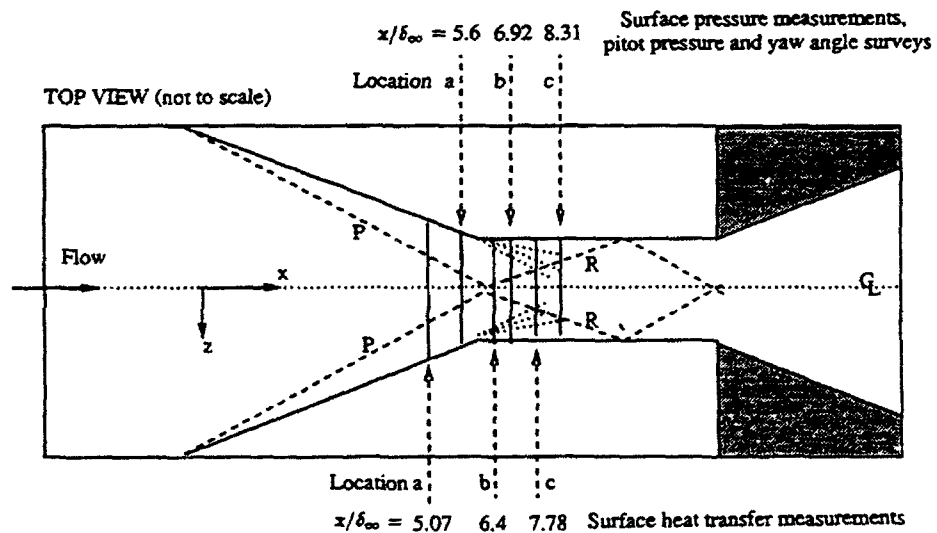


Fig.2 Locations of experimental measurements

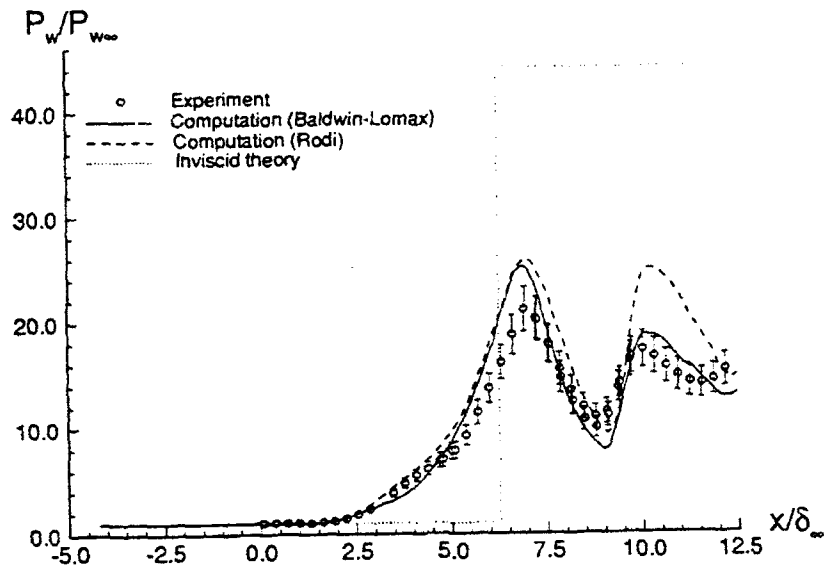


Fig.3 Flat plate surface pressure along centerline.

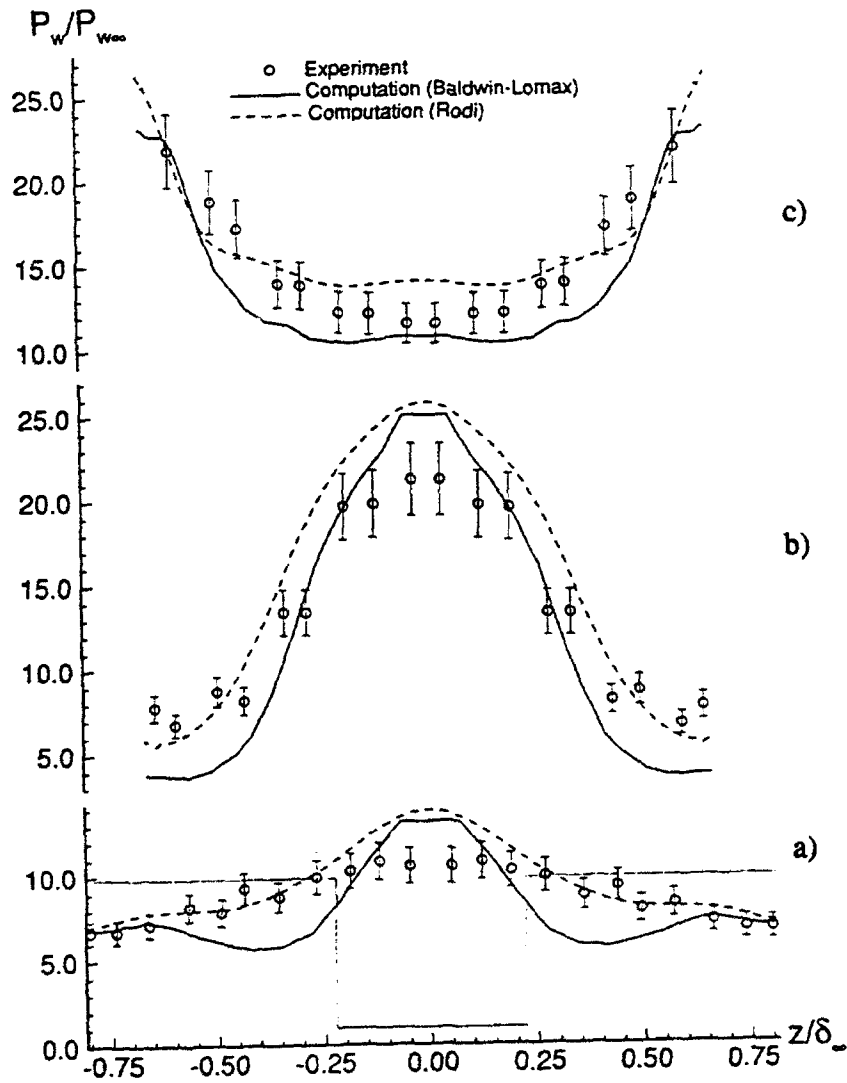


Fig.4 Transverse profiles of flat plate surface pressure at streamwise locations of (a)  $x/\delta_{\infty} = 5.6$ , (b)  $x/\delta_{\infty} = 6.92$  and (c)  $x/\delta_{\infty} = 8.31$ .

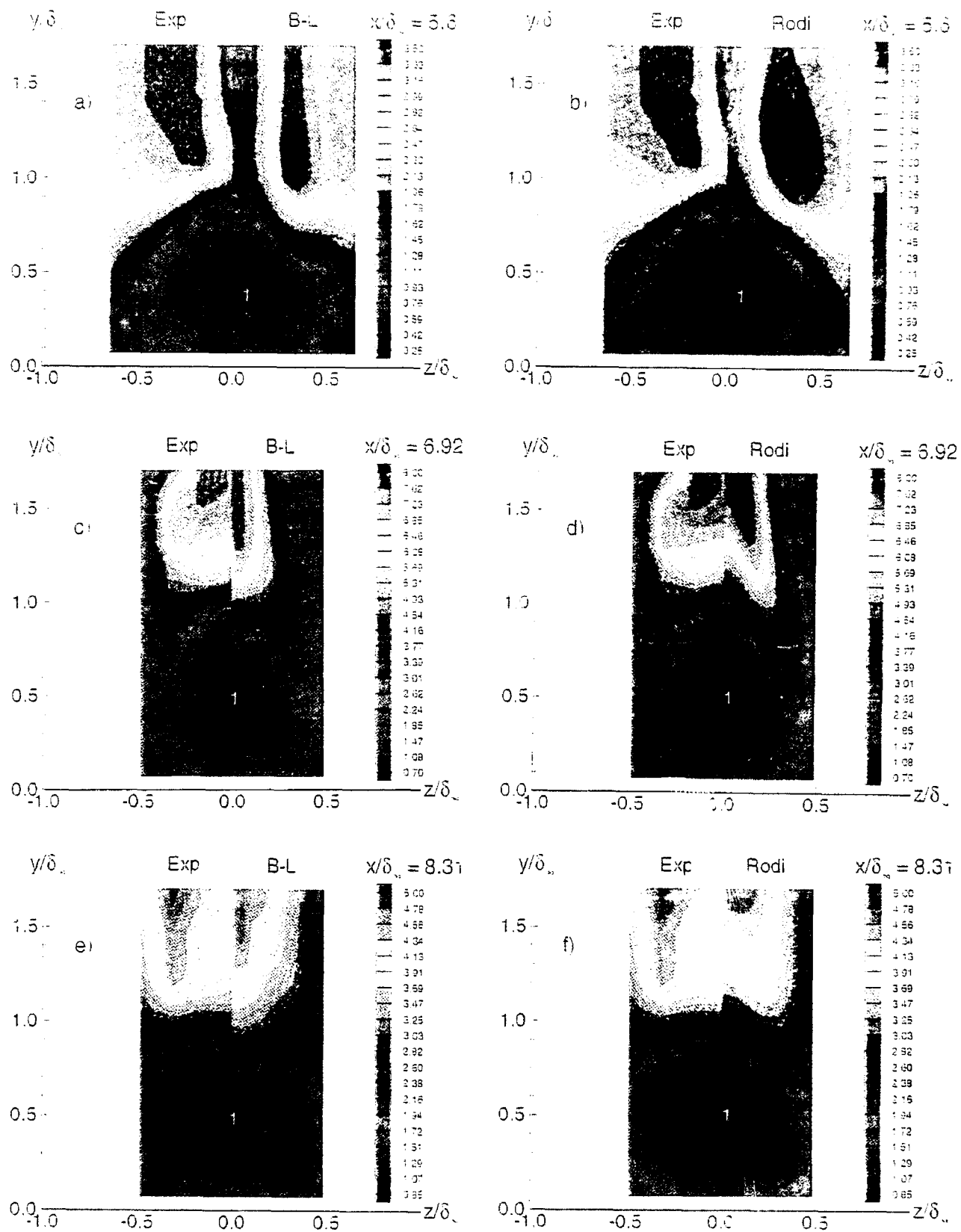
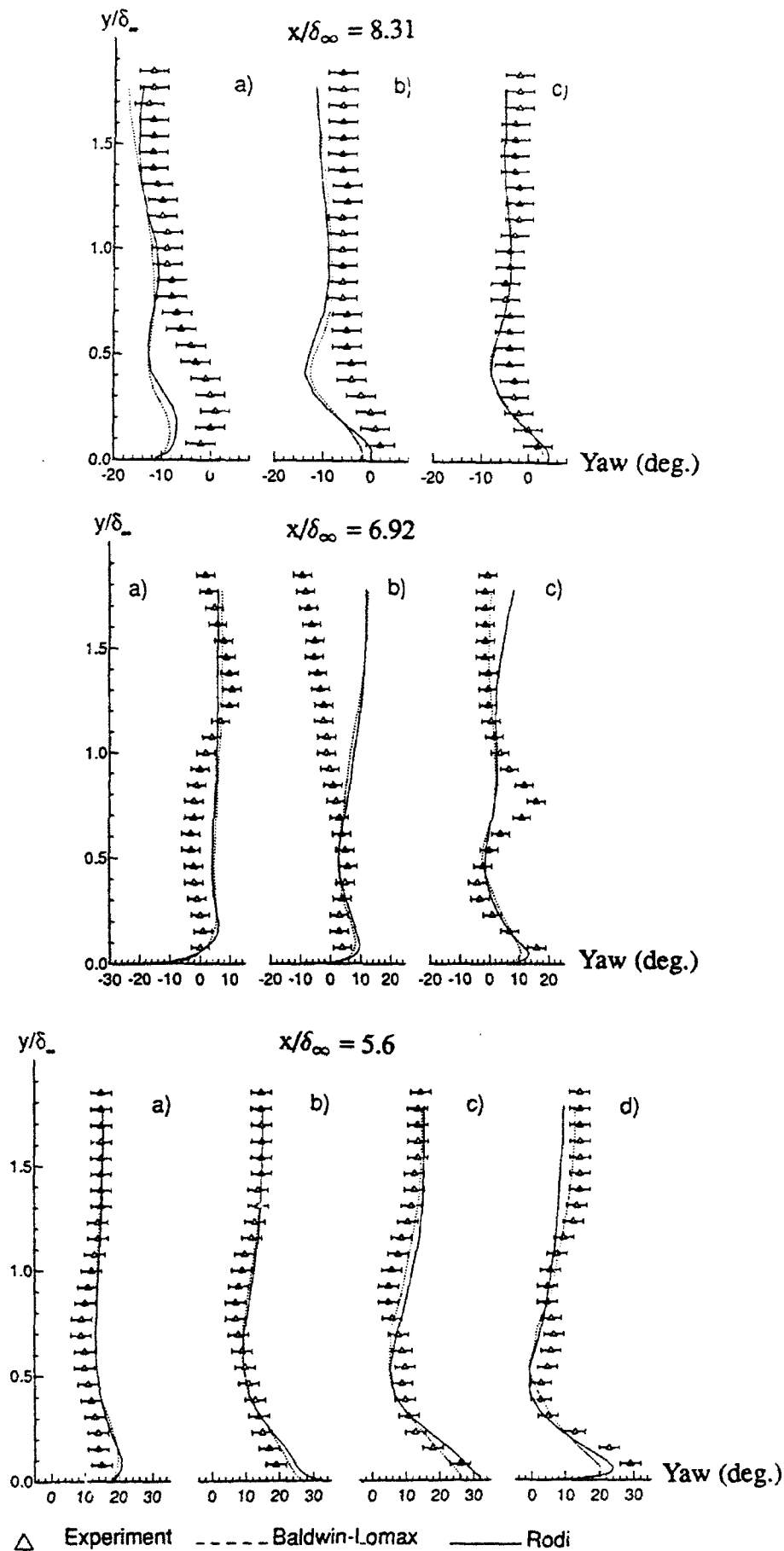


Fig.5 Experimental and computed pitot pressure ( $P_p/P_{p\infty}$ ) on cross-flow planes at (a,b)  $x/\delta_\infty = 5.6$ . (c,d)  $x/\delta_\infty = 6.92$  and (e,f)  $x/\delta_\infty = 8.31$ . Legend : 1 = low total pressure jet.



**Fig.6** Experimental and computed yaw angle profiles (in deg.) at  $x/\delta_\infty = 5.6$  (locations a-d are at  $z/\delta_\infty = -0.65, -0.49, -0.33$  and  $-0.16$ ),  $x/\delta_\infty = 6.92$  (locations a-c are at  $z/\delta_\infty = -0.48, -0.32$  and  $-0.15$ ), and  $x/\delta_\infty = 8.31$  (locations a-c are at  $z/\delta_\infty = -0.48, -0.32$  and  $-0.15$ ). Note :  $z/\delta_\infty = 0.0$  is centerline.

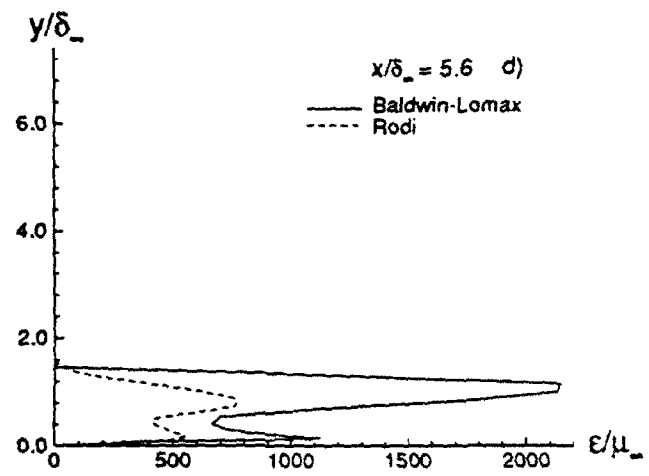
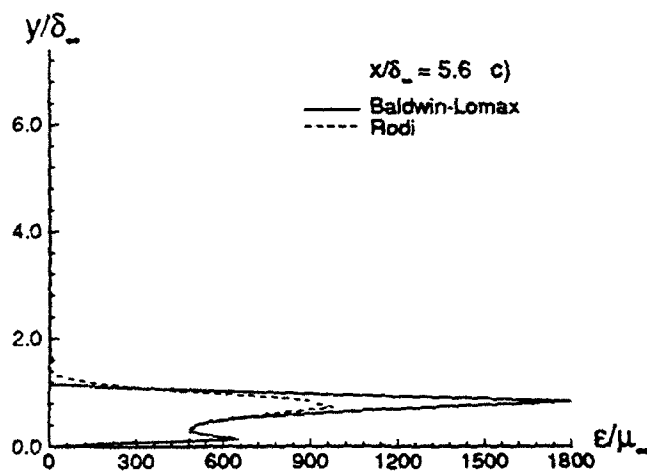
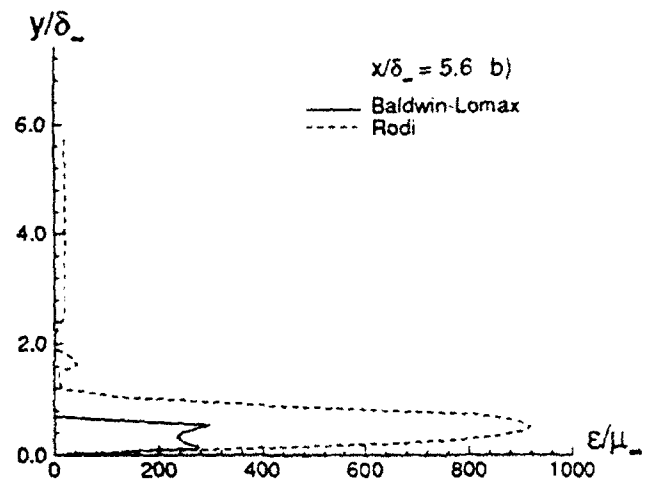
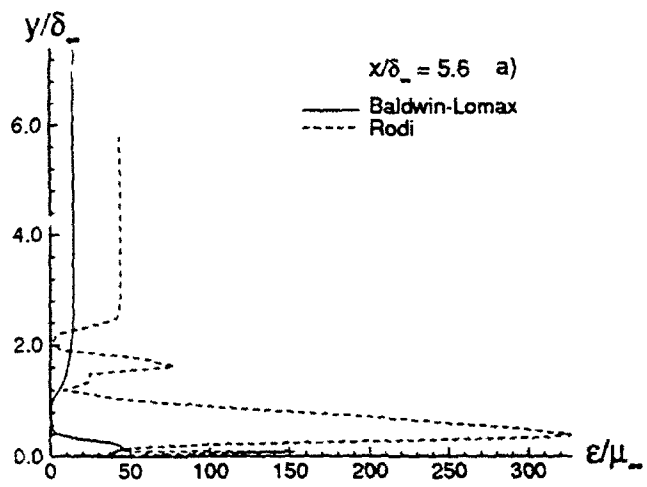


Fig.7 Computed eddy-viscosity profiles at  $x/\delta_\infty = 5.6$ . Locations a-d are at  $z/\delta_\infty = -0.65, -0.49$  and  $-0.33$  and  $-0.16$ . Note :  $z/\delta_\infty = 0.0$  is centerline.

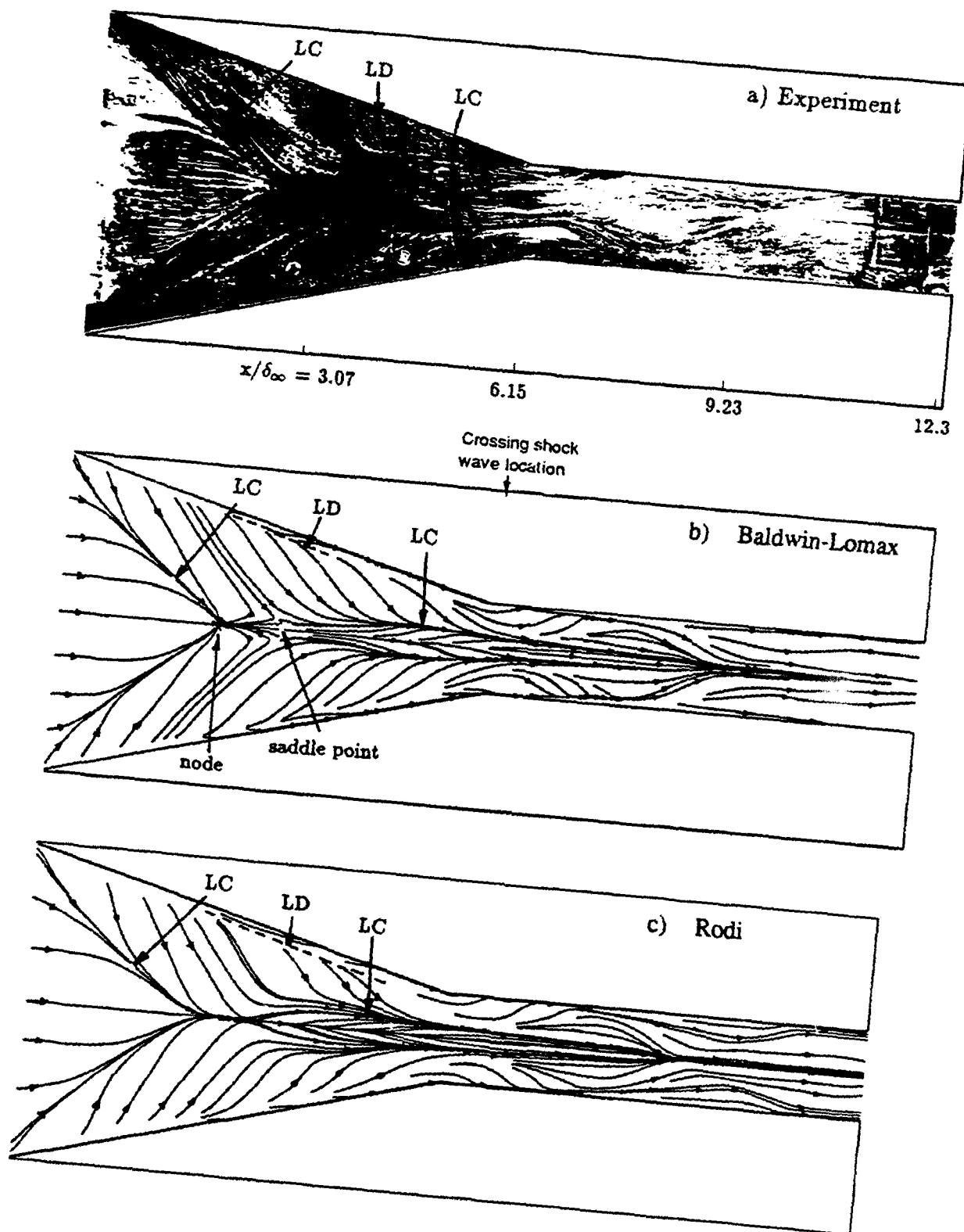


Fig.8 Surface flow pattern: (a) = experiment, (b) = Baldwin-Lomax computation, (c) = Rodi computation

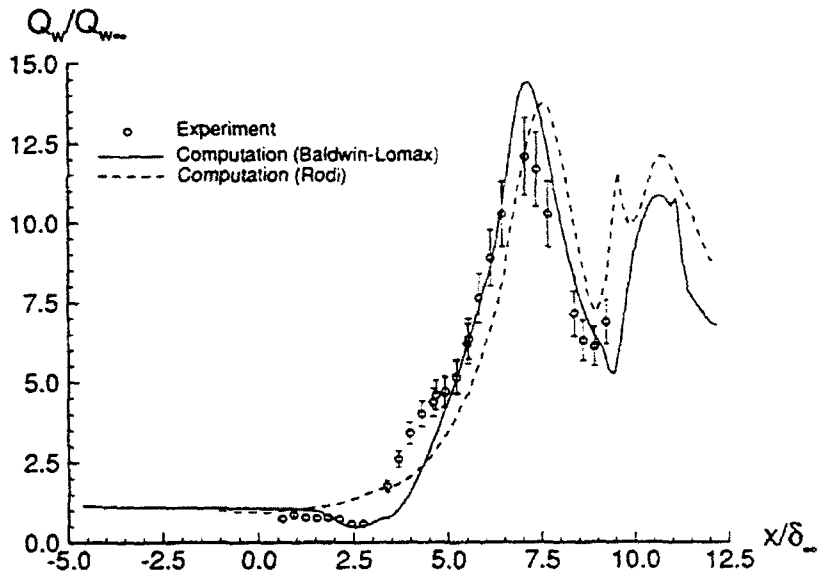


Fig.9 Flat plate surface heat transfer along centerline.

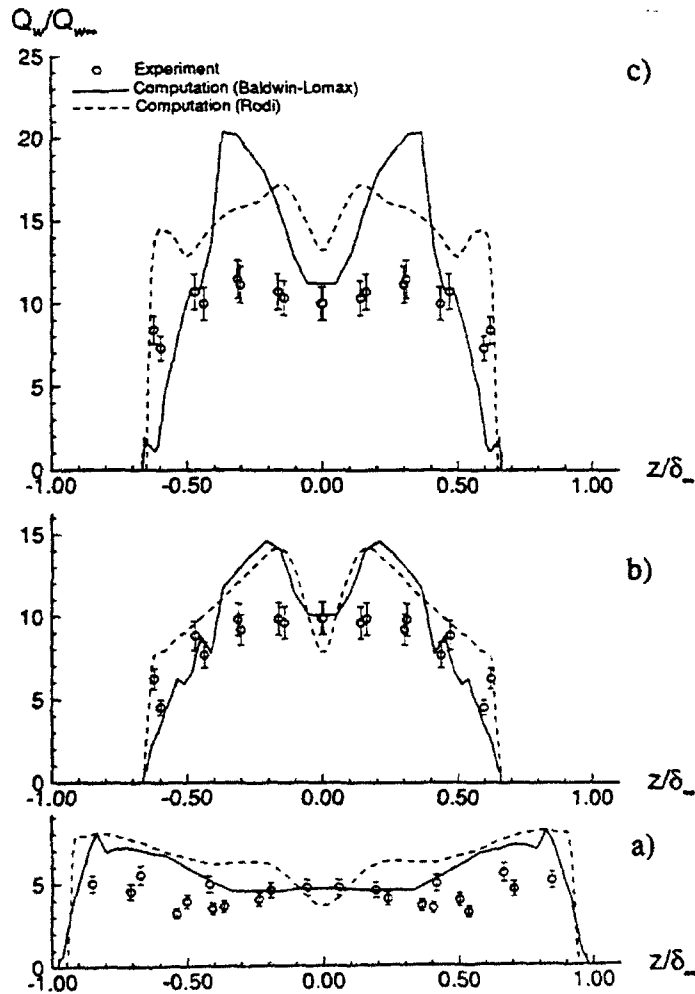
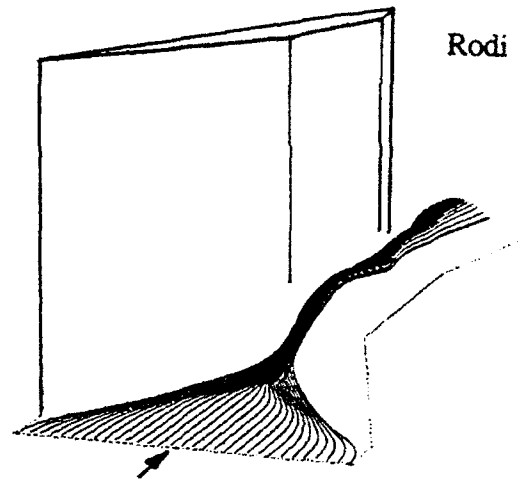
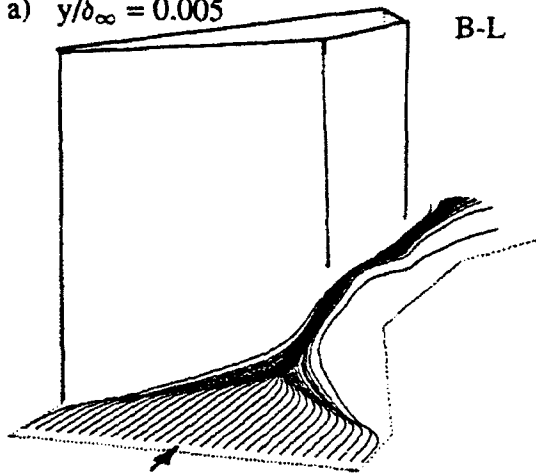
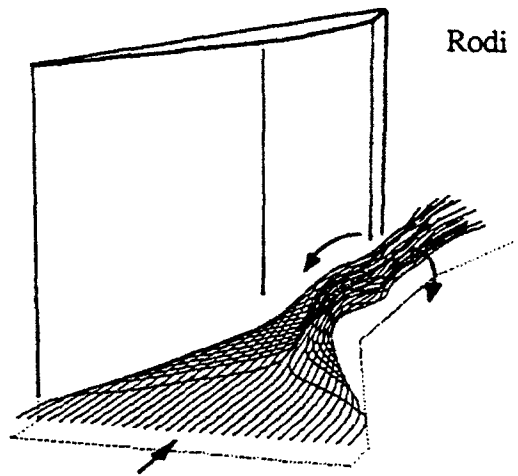
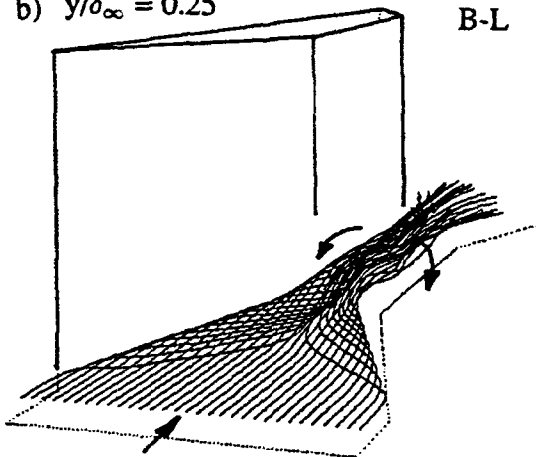


Fig.10 Transverse profiles of flat plate surface heat transfer at streamwise locations of (a)  $x/\delta_\infty = 5.08$ , (b) 6.4 and (c) 7.78.

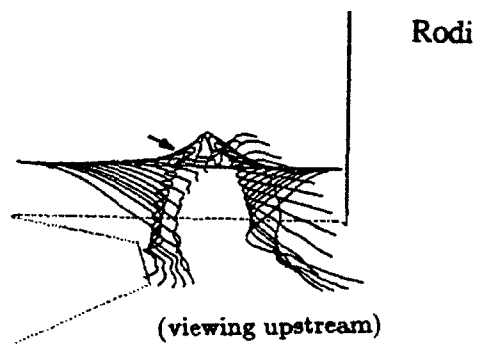
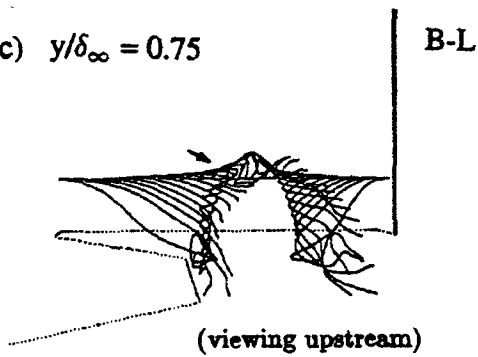
a)  $y/\delta_\infty = 0.005$



b)  $y/\delta_\infty = 0.25$



c)  $y/\delta_\infty = 0.75$



d)  $y/\delta_\infty = 1.0$

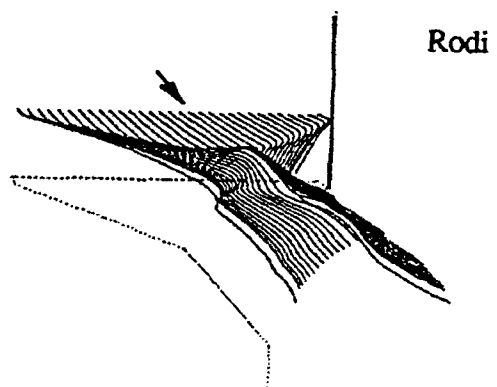
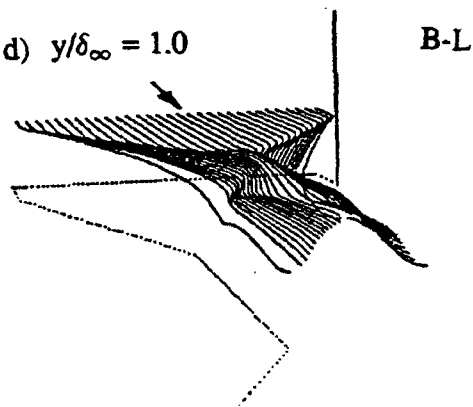


Fig.11 Streamlines originating from various  $y/\delta_\infty$  levels in the upstream boundary layer.

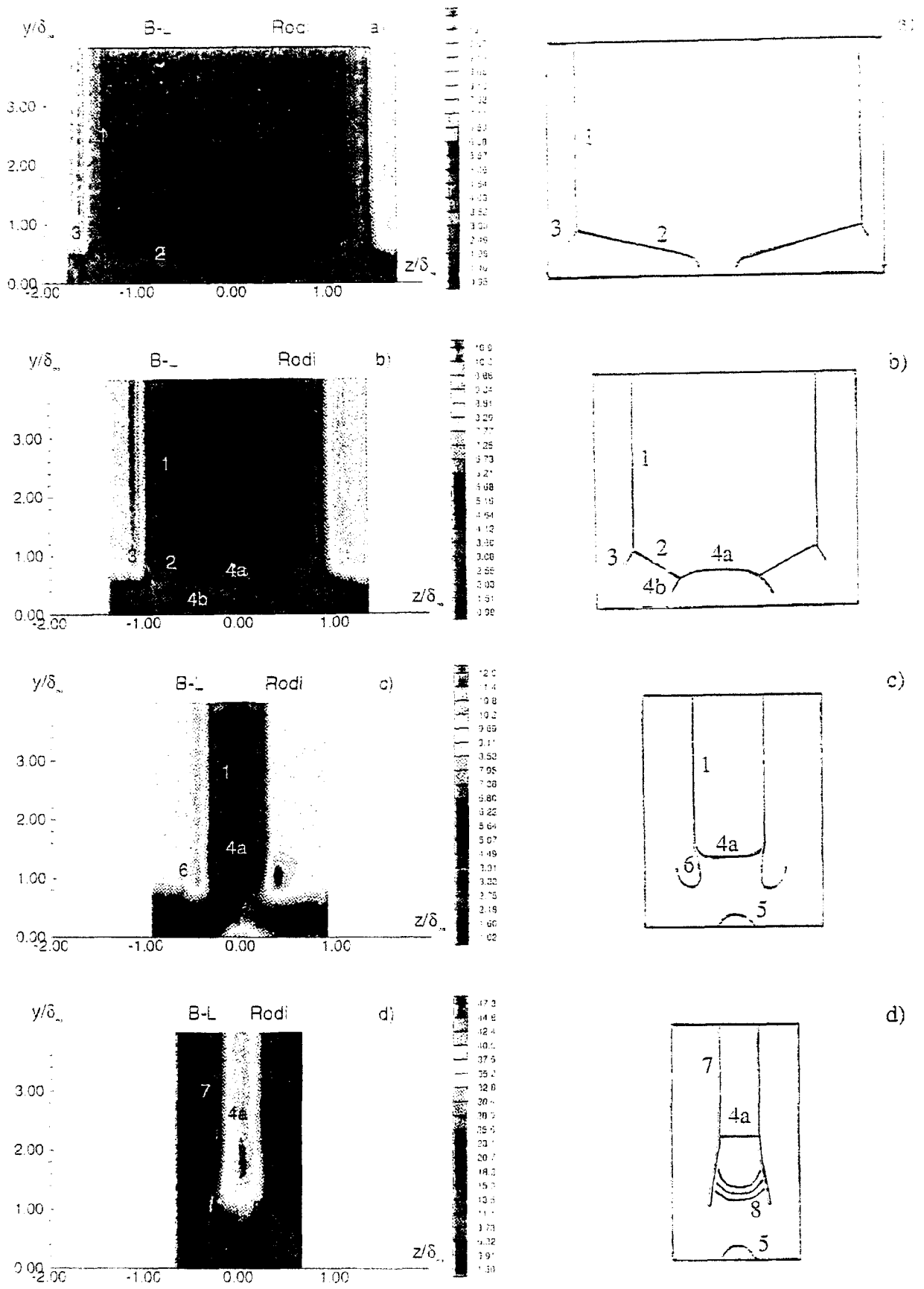


Fig.12 Computed static pressure contours on cross-flow planes at (a)  $x/\delta_\infty = 2.15$ , (b)  $x/\delta_\infty = 3.57$ , (c)  $x/\delta_\infty = 5.23$ , (d)  $x/\delta_\infty = 7.38$ . Schematics are shown alongside.

**Attachment No. 2**

**"Structure of Crossing Shock Wave - Turbulent Boundary Layer  
Interactions"**

by T. J. Garrison, G. S. Settles, N. Narayanswami and D. D. Knight

presented at the AIAA/SAE/ASME/ASEE 28th Joint Propulsion  
Conference, July 1992, Nashville, TN



**AIAA-92-3670**

**Structure of Crossing-Shock Wave/  
Turbulent Boundary-Layer Interactions**

T. J. Garrison and G. S. Settles

Penn State University, University Park, PA;

N. Narayanswami and D. D. Knight

Rutgers University, Piscataway, NJ

**AIAA/SAE/ASME/ASEE  
28th Joint Propulsion  
Conference and Exhibit  
July 6-8, 1992 / Nashville, TN**

## Structure of Crossing-Shock Wave/Turbulent Boundary-Layer Interactions

T.J. Garrison\* and G.S. Settles\*\*  
 Penn State University, University Park, PA;  
 N. Narayanswami† and D.D. Knight‡  
 Rutgers University, Piscataway, NJ

### Abstract

A detailed comparison of experimental and computational results on the flowfield structure of a Mach 4, 15 degree symmetric crossing-shock wave/turbulent boundary layer interaction is presented. Experimentally obtained Planar Laser Scattering images are compared with static pressure contours predicted by the computation, with the computational results showing good overall agreement with the experimental data. The experimental and computational results are used in a complementary manner to develop a detailed flowfield model of the crossing shock interaction. The flowfield structure is found to consist of a complex shock structure overlying a large viscous separated region. This region occupies a significant portion of the outflow duct and consists of an accumulation of low-Mach-number, low-stagnation-pressure fluid. This region may have significant implications for sidewall compression inlets.

### Introduction

The interactions between shock waves and turbulent boundary layers are very practical propulsion-related problems, especially in association with engine inlets. These complex viscous/inviscid interactions occur in virtually all high speed inlets, and play a key role in determining the quality of the flow within the engine. Thus, a fundamental understanding of the physics of these interactions is critical to the design of efficient propulsion systems.

Over the past fifty years a great deal of research has been directed toward understanding shock/boundary layer interactions, its emphasis being geared toward 2-D and "simple" 3-D flows (see Ref. 1 for a thorough review of these research efforts). More recently, effort has been focused on understanding more complex, fully-three-dimensional interactions. One particular example is the

crossing-shock wave/boundary layer interaction (Fig. 1). The crossing-shock interaction is comprised of the confluence of two separate single-shock interactions (for which a great deal is already known), and thus represents a logical progression in the study of shock/boundary layer interactions. This interaction also applies to propulsion systems, since many high-speed inlets use sidewall compressions similar in geometry to the model shown in Figure 1.

Current research on crossing-shock interactions is divided almost evenly between experimental and computational efforts. Early experimental efforts [2-6] focused mainly on characterizing the surface flow features, with emphasis on wall static pressure and streamline patterns. More recently, experimental efforts have gained an understanding of the overall flowfield structure and developed a physical model of these complex interactions [7,8]. Computational predictions of crossing-shock interactions have been performed by several investigators [9,10], but until recently have had only limited experimental data with which to compare, making a conclusive evaluation of the computations impossible. Thus, there is a need to compare the newly-acquired experimental data with the computational predictions.

The goal of this paper is to present a detailed comparison of experimental and computational results for a common interaction, examining both the surface features and the flowfield structure above the surface. The objectives of this comparison are to evaluate the ability of the computation to predict the flowfield, and to improve and revise the flowfield model originally presented in Ref. 7. By comparing the results of the data and the prediction, the strengths of both are used in a complementary fashion to formulate a detailed flowfield model of the crossing-shock interaction.

### Description of Experiments

The experiments were performed in the Penn State Gas Dynamics Laboratory's Supersonic Wind Tunnel Facility, which is an intermittent blowdown tunnel with a test section size of 15x17x60 cm. This facility has a unique variable Mach number capability over the range from Mach 1.5 to 4.0. For the experiments described in this paper, typical tunnel operating conditions were a stagnation pressure of 1500 KPA, a stagnation temperature of 295 K, and a unit Reynolds number of 76 million /meter.

Figure 1 shows the model geometry used for the crossing-shock experiments. This model consists of two vertical

\* Graduate Research Assistant, Mechanical Engineering Dept.  
 Student Member AIAA.

\*\* Professor of Mechanical Engineering and Director, Gas Dynamics Laboratory. Associate Fellow AIAA.

† Research Staff Member, Mechanical and Aerospace Engineering Dept., Student Member AIAA.

‡ Professor of Mechanical and Aerospace Engineering.  
 Associate Fellow AIAA.

Copyright © 1992 by the American Institute of Aeronautics and Astronautics, Inc.

fins, both at angle of attack  $\alpha$ , mounted to a horizontal flat plate. The flat plate generates an equilibrium, nearly adiabatic, zero-pressure-gradient turbulent boundary layer which interacts with the two crossing oblique shock waves generated by the fins. The incoming properties of the boundary layer are  $\delta \approx 3.5$  mm,  $\delta'' \approx 1.12$  mm, and  $\theta \approx 0.13$  mm (values revised from Ref. 7). The fins are located 21.3 cm downstream of the plate leading edge, with a transverse distance between the fin leading-edges of 9.63 cm. The height of the fins is 8.25 cm, large enough to be effectively "semi-infinite".

The complete experimental program examined a range of symmetric shock generator angles ranging from 7 to 13 degrees at Mach 3 and 7 to 15 degrees at Mach 4. However, this paper will focus on the analysis of only one case, namely the Mach 4, 15 degree interaction. The experimental measurements consisted of surface flow visualization and Planar Laser Scattering (PLS) flowfield visualization. PLS visualization, also referred to as laser light screen or vapor screen visualization, is a technique by which the details of a flowfield can be recorded through scattering of laser light by seed particles in the flow. A more detailed description of the experimental setup and techniques is given in Ref. 7.

#### Description of Computations

A computation of the Mach 4, 15 degree interaction was performed for the same flow conditions as the experimental case, but with a slightly modified geometry. Referring to Figure 1b, in the experiment the fins were terminated at a distance  $Z=Le$  downstream from the fin leading edges, where  $Le$  is the distance required for the inviscid shocks to intersect the opposite fin surfaces. To simplify the body-fitted grid system, the physical domain of the computation was modified by the addition of an outflow duct of angle  $\theta=30^\circ$ . The effect of this modification on the flowfield region of interest (i.e. the region surrounding the crossing shocks) is believed to be negligible, since there is supersonic flow over the entire computational domain at  $Z=Le$ .

The theoretical model used in the computation is the full 3-D mean compressible Reynolds-averaged Navier-Stokes equations in strong conservation form [11]. Turbulence is incorporated through the Baldwin-Lomax [12] algebraic eddy-viscosity model. The numerical algorithm employed is the hybrid explicit-implicit scheme of Knight [13]. Utilizing the symmetry of the crossing-shock interaction, the physical domain in the computation is reduced to one-half of the experimental domain.

Boundary conditions employed for the computational domain are as follows:

- On the inflow boundary, an incoming 2-D equilibrium turbulent boundary layer profile is prescribed to match the experiment.
- On the fin and plate surfaces, the velocity vector and normal gradient of static pressure are set to zero. The wall temperature is set to  $1.06 T_{aw}$ , to match the experimental value.
- On the plane of symmetry, the normal component of

velocity is set to zero, as are the normal gradients of static pressure, temperature, and the remaining two velocity components.

- On the top and outflow boundaries, the gradient of all flow variables is set to zero.

For simplicity in the computational solution, the fin boundary layer is taken to be turbulent from the leading edge. Although this differs from the experiment, for which the transition point occurs downstream of the leading edge, the effect of this assumption on the flowfield region of interest has been shown to be negligible in past analysis of single fin interactions [14,15].

Details of the computational grid used are given in Table 1. The grid spacings are comparable to or better than those employed in previous single fin [14,15] and crossing shock computations [9]. A non-uniform grid spacing in the Z direction is used, with the minimum grid spacing located in the region near the inviscid shock crossing. The computation was performed on a CRAY Y-MP (single processor) and required approximately 32 hours of CPU time.

#### Comparison of Results

##### Surface Streamline Patterns

Figure 2 shows a comparison of experimental and computational surface streamline patterns. It should be noted that the experimental pattern is not for the Mach 4, 15 degree interaction but rather for a weaker case (Mach 3, 11 degree interaction). The reason for this is that, for very strong interactions, the fins must be positioned at angle of attack after the windtunnel has started, resulting in lower quality traces which are not very reproducible. However, the features shown in the experimental trace of Figure 2 are typical of the interactions examined experimentally, and can be compared qualitatively with the computational pattern.

Examination of the results given in Figure 2 shows that upstream, near the fin leading edges, the patterns are quite similar, as would be expected since the interaction starts as two separate single fin interactions for which a great deal of research has been done. Evident in both figures are the primary separation and attachment lines and the line of upstream influence. Moving downstream, differences in the two patterns become evident, especially near the interaction centerline. In the computation, the primary separation lines come together at the interaction centerline, forming a node of attachment, while in the experimental trace the separation lines initially converge toward the centerline but then turn downstream, never actually merging together. In fact, all the experimental traces recorded over a range of interaction strengths showed this same behavior: the primary separation lines initially converge toward the centerline, then diverge from it, then finally approach it again further downstream. The discrepancies in the computational and experimental patterns along the interaction centerline are most likely attributable to the inaccuracy of the Baldwin-Lomax turbulence model used in the computation. This region consists of a highly separated, vortical flowfield which is quite complex and most likely not

modeled well near the surface. Away from the centerline, the computed patterns again show reasonable agreement with the experimental results.

Based on a comparison of the computed and experimental flowfields above the surface, as described in the following section, it is felt that the flowfield features in the vicinity of the interaction centerline are very localized near the plate surface and do not have a significant effect on the flowfield away from the surface. However, the effects on surface properties such as skin friction and heat transfer are yet to be fully resolved. Experimental heat transfer measurements for a Mach 8.3, 15 degree interaction [8] reveal a relatively flat  $C_f$  distribution across the centerline, which may indicate that the observed features are not very significant to the surface properties either. Experimental skin friction measurements for a range of cases are currently underway at Penn State, and these results should shed more light on the significance of the surface flow features near the interaction centerline.

### Wave Structure

Figure 3 shows a comparison of computed values of the normalized static pressure,  $P/P_\infty$ , with the experimentally recorded Planar Laser Scattering images at 14 spanwise planes throughout the interaction (note that the color scale for the computational results has been optimized for each frame, resulting in a variable color scale as indicated in the legends of Fig. 3). These frames are at equally spaced intervals of  $Z/\delta_\infty = 1.43$  with the first frame at  $Z/\delta_\infty = 16.6$ . The origin of the  $Z$  axis is on the interaction centerline at the fin leading edge position, as indicated in Fig. 1b. Figure 4 shows a corresponding interpretation of the key features revealed in the images of Figure 3, and will be used as a basis for discussion of the flowfield structure. Also shown in Figure 4 is a schematic depicting the locations of the 14 frames relative to the model geometry. Notice that, based on the inherent symmetry of the crossing shock interaction, only half of the actual interaction is shown in Figure 4. Also, it should be noted that the images shown in Figure 3 are at 1.3 times full scale, while the schematics of Figure 4 are to actual scale. Finally, much of the discussion of the shock wave structure which follows relies on the detailed analysis originally given in Reference 7, and this reference should be consulted if additional insight is required.

Frames a) of Figures 3 and 4 occur upstream of where the two single fin interactions meet, and thus represent two separate single fin interactions. The main, separation, and rear shocks are visible in both the experimental and the computational results (note that due to a restricted field of view the PLS images do not extend out to the fin surfaces). Also visible in the experimental images is the separation bubble under the bifurcated shock system, appearing as the dark region near the plate surface. This separated region does not show up well in the computational plots of static pressure, but does appear clearly in plots of total pressure, such as the one shown in Frame o). In general, the size and

shape of the computed separated region compares quite well with the experimental results throughout the interaction. However, because the static pressure plots reveal the shock structure best, they alone are presented in the remaining frames of Fig. 3 for brevity.

Frame b) occurs slightly downstream of where the two separation shocks meet. To understand the confluence of these two separate single-fin interactions, it is beneficial to make use of the method originally presented in Ref. 7. Here, the  $Y-Z$  plane passing through the interaction centerline is considered an inviscid reflection plane. Because of the inherent symmetry of the crossing-shock interaction, shock waves which intersect this plane must reflect off it in order to satisfy continuity. With this reference frame, we see that the incident separation shock reflects from the reflection plane, appearing as a bright region in the PLS images on the interaction centerline near the plate surface. The high static pressure region associated with this "reflected" separation shock can also be seen in the computational image, which coincides well with the experimental result. Frames c) through e) show that the incident separation shock continues to "reflect" off the reflection plane, with the corresponding image of the shock in the experimental PLS images comparing quite well to the high static pressure region in the computation.

Frame e) occurs approximately at the location where the reflected separation shock crosses the incident rear shock. Up to this point, the experimental and computational results compare quite well. However, beyond frame e) a significant difference in the two results becomes evident. In the experimental PLS images of frames f) and beyond, it is observed that the reflected separation shock crosses through the incident rear shock and continues outward toward the fin, while in the computational results, beyond frame e) the reflected separation shock is no longer seen (i.e. following the terminology of Frame j, the main segment of the reflected separation shock, 6c, is not present in the computational solution). Examination of the experimental images in Figure 3 clearly shows the presence of the feature which has been labelled as the main segment of the reflected separation shock in Figure 4. Furthermore, experimental surface flow visualization traces on the fin show the intersection of this shock wave with the fin well in front of the location at which the inviscid shock intersects the fin, as can be seen from Figure 5. (This fin trace is for a weak interaction, Mach 3, 9 degrees, but the same pattern was observed for all interactions examined.) In addition, the feature observed on the fin cannot be associated with the inviscid shock wave, since it occurs near the plate surface and the inviscid shock segments end well above the plate surface. Thus, it is felt that the main segment of the reflected separation shock is definitely present in the experiment, but appears to be absent in the computation. Further research effort is needed to resolve this discrepancy, possibly by repeating the computation with a significantly reduced grid size.

Next, Frame g) occurs just upstream of the inviscid shock crossing location. The static pressure plots reveal the formation of two high pressure regions located symmetrically about the reflection plane. It is believed that these regions are associated with the complex shock crossings which occur as the two inviscid shock waves approach one another. Just below the triple point, the bifurcated shock system reflects from the reflection plane, resulting in the reflection of the incident separation shock, the crossing of this reflected separation shock by the incident rear shock, and finally the reflection of the incident rear shock. This complex sequence of reflections and crossings occurs over a relatively short streamwise distance. However, at present neither the experiment nor the computation has the resolution to adequately resolve the details of this section of the interaction. Based on the experimental images, it is believed that the incident  $\lambda$  shock structure reflects from the centerplane and remains intact, though somewhat distorted, propagating back outward toward the fin surface. Current experiments are underway at Penn State to examine the nature of the crossing region in greater detail in order to better understand the complex sequence of events associated with the crossing of the bifurcated shock system.

In Frame i), which is downstream of the inviscid crossing point, the reflected separation shock becomes distorted as it propagates into regions of varying Mach number. Referring to Frame j), the portion of this reflected separation shock which propagates upward between the two inviscid shocks has been labelled as the centerline segment, 6a. This segment of the reflected separation shock is resolved by the computation, unlike the main segment discussed previously. Relative to the freestream flow direction, the centerline shock segment is inclined at a steeper angle than the main segment, due to the substantially reduced Mach number in the region between the crossed inviscid shocks. Consequently, this shock segment "propagates" upward much faster than the main segment of the reflected separation shock approaches the fin. This leads to the formation of a "bridge" shock segment, 6b, which connects these two shocks, thus maintaining a continuous shock front and producing an additional triple point where the bridge and centerline segments meet the inviscid shock.

In Frames h) and beyond, the high centerline static pressure region predicted by the computations corresponds quite well with the shock envelope comprised of the centerline and bridge segments of the reflected separation shocks and the reflected rear shock (i.e. shocks 6a, 6b, and 7). This envelope continues to grow in size as the reflected shock system moves outward toward the fin. In addition, the shape of the inviscid and bridge shock segments (8 and 6b) show good agreement with the shape of the main shock structure predicted by the computation. The computation also reveals the development of an expansion region located between the two inviscid shocks, just above the separated region (this expansion is especially evident in Frames k and beyond). This expansion cannot be seen in the experimental images because the PLS technique cannot resolve such

diffuse gradients as those associated with a weak expansion.

### Streamline Structure

Up to this point it has been easiest to take features found in the experimental images and find the corresponding features in the computation, simply because the resolution of the PLS images is much better than that of the computation. However, due to high temperatures and low densities which greatly reduce the seeding density, the experimental PLS images can only resolve the size and shape of the separated region, but not the actual details within it. One expects the presence of two vortical structures (cf [9,16]), arising from the two original single-fin interactions, and based on this expectation the locations of the vortices within the separated region were estimated in the original flowfield model given in Ref. 7. Based on the comparison in the previous section it was established that the computational solution does a reasonable job of predicting the flowfield structure. Thus, the computational solution may now be used to provide additional detail in this region. It shows that the vortices are actually located closer to the plate surface than originally estimated in Ref. 7. The cores of these vortices show up clearly in the computations as two low-static-pressure regions near the plate surface. Also revealed by the computation is the presence of a very high static pressure region between these vortices. This feature does show up in the experimental PLS images, appearing as a brighter region at the plate surface near the interaction centerline. At present, the physical mechanism responsible for this high pressure region is not completely understood.

Computational particle traces within the flowfield can also be used to help understand the flowfield streamline structure, especially within the separated region. By releasing particles at various distances from the flat plate surface within the incoming boundary layer, the flowfield streamlines can be determined. Figure 6 shows a sequence of traces for particles originating at  $y/\delta_{in} = 0.01, 0.25,$  and  $1.0$ . From these traces, the formation of two counter-rotating vortices can clearly be seen. These vortices are formed in association with the two single fin interactions and converge upon the centerline as the two interactions cross. It can also be seen that essentially the entire incoming boundary layer along with fluid originating in the freestream flow becomes engulfed into the separated region. This results in the accumulation of a large low-Mach-number, low-stagnation-pressure region which occupies a significant portion of the outflow duct. Since the desired output of an inlet is a uniform, high-stagnation-pressure flow, this large separated-flow region has significant implications in the design of high-speed engine inlets.

Figure 6 also shows that the two vortices initially lift upward rapidly as they approach one another and then tend to "level off" further downstream. This levelling-off of the streamlines within the separated region is consistent with the observation of the expansion above the separated region, as discussed in the previous section.

A clearer view of the twin vortices in this symmetrical interaction is shown in Figure 7, where the particle paths seen in Fig. 6 are now viewed from downstream. In Fig. 7a the rollup of vorticity from the entire incoming boundary layer between the fin leading-edges is clearly shown to result in two concentrated vortex cores. In Fig. 7b (viewed in a direction exactly opposite to that of the freestream) the locations of these twin vortex cores are revealed.

Outside of the separated region, a new boundary layer forms through reattachment of fluid originating outside the incoming boundary layer. This results in the formation of a very thin boundary layer, for which large gradients and potentially high skin friction and surface heat transfer rates may be expected (Fig. 6c). Experiments are underway to examine the skin friction distribution both along the interaction centerline and in the spanwise direction for a range of crossing shock interactions. The results of these experiments should shed more light on these interactions, and also provide a stringent test for the computations. Past experience has shown the prediction of skin friction to be a major limitation in computations of these complex interactions, most likely attributable to the turbulence models.

### Conclusions

The flowfield structure of a symmetric crossing-shock/turbulent boundary layer interaction is examined both experimentally and computationally. The computation is shown to give reasonable agreement with the experimental data, with two significant differences. The surface pattern predicted by the computation does not agree with the experiment in the vicinity of the interaction centerline, with the difference being attributable to the turbulence model. Also, the computation fails to resolve the presence of the main segment of the reflected separation shock. This discrepancy is not understood, but may be due to resolution limits of the computation.

The results of the two analyses are used in a complementary manner to develop a revised model of the flowfield structure. The experiments provide good resolution of the shock structure and show that the incoming bifurcated shock structures originating from the two separate single fin interactions cross through one another, becoming somewhat distorted, but maintaining their  $\lambda$ -shaped structure. The computations provide insight into the nature of the separated flow region, showing the presence of two counter-rotating vortices and the accumulation of a large, low-momentum region which may be highly detrimental to high-speed sidewall-compression inlets.

### Acknowledgements

This work was supported by AFOSR under Grants 89-0315 and 86-0266, monitored by Dr. Len Sakell. Supercomputing time was provided at the National Center for Supercomputing Applications by Cray Research Inc. through the 1992 University Research and Development Grant.

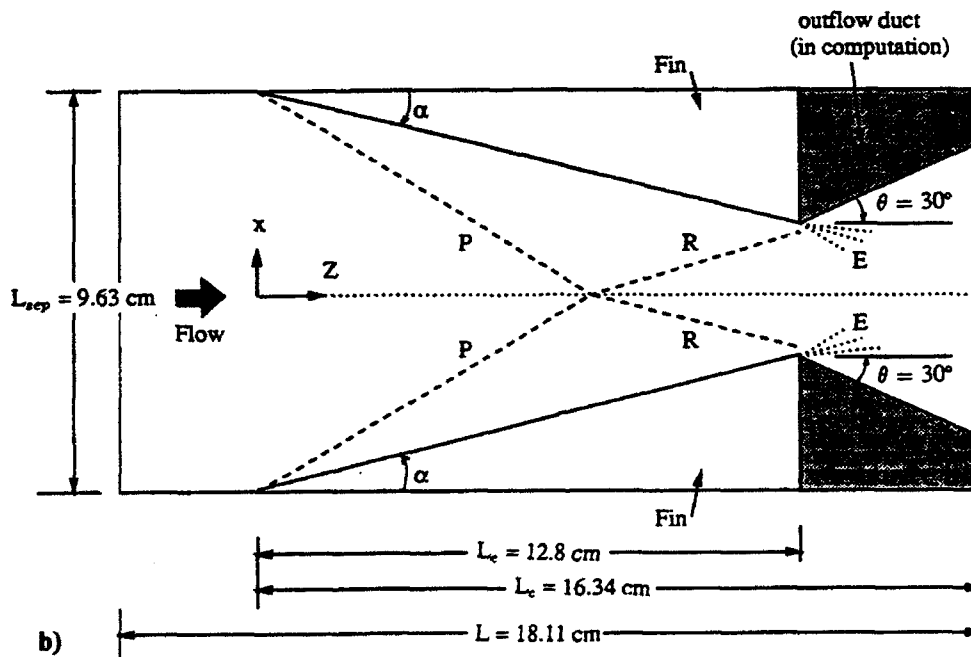
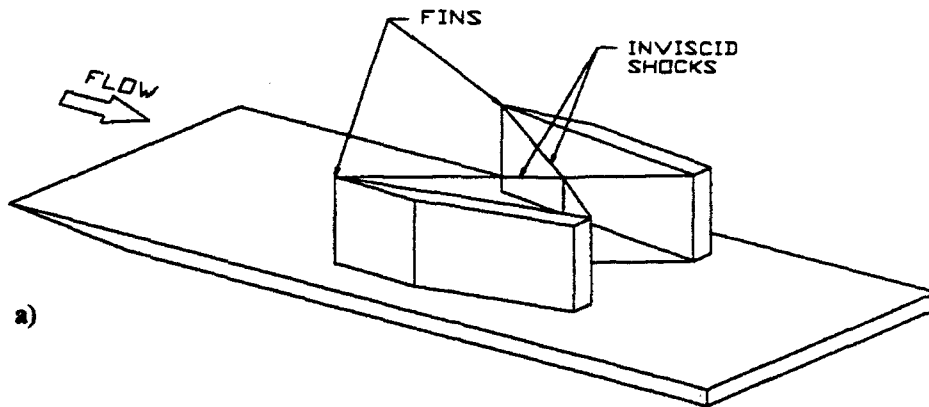
### References

- [1] Settles, G.S. and Dolling, D., "Swept Shock/Boundary Layer Interactions - Tutorial and Update," AIAA Paper 90-0375, Jan. 1990.
- [2] Batcho, P.F., Ketchum, A.C., Bogdonoff, S.M. and Fernando, E.M., "Preliminary Study of The Interactions Caused by Crossing Shock Waves and a Turbulent Boundary Layer," AIAA Paper 89-0359, Jan. 1989.
- [3] Poddar, K. and Bogdonoff, S.M., "A study of the Unsteadiness of Crossing Shock Wave Turbulent Boundary Layer Interactions," AIAA Paper 90-1456.
- [4] Mee, D.J., Stalker, R.J., and Stollery, J.L., "Glancing Interactions Between Single and Intersecting Oblique Shock Waves and a Turbulent Boundary Layer", *Journal of Fluid Mechanics*, Vol. 170, 1986, pp. 411-433.
- [5] Hingst, W.R., and Williams, K.E., "Interaction of Two Glancing, Crossing Shock Waves with Turbulent Boundary Layers at Various Mach Numbers," NASA TM 103740.
- [6] Bogdonoff, S.M., and Stokes, W.L., "Crossing Shock Wave Turbulent Boundary Layer Interactions - Variable Angle and Shock Generator Length Geometry Effects at Mach 3", AIAA Paper 92-0636, Jan. 1992.
- [7] Garrison, T.J. and Settles, G.S., "Flowfield Visualization of Crossing Shock-Wave/Boundary Layer Interactions," AIAA Paper 92-0750, Jan. 1992.
- [8] Kussoy, M.I., and Horstman, K.C., "Intersecting Shock-Wave/Turbulent Boundary-Layer Interactions at Mach 8.3," NASA TM 103909, 1992.
- [9] Narayanswami, N., Knight, D., Bogdonoff, S.M., and Horstman, C.C., "Crossing Shock Wave-Turbulent Boundary Layer Interactions," AIAA Paper 91-0649, accepted for publication in *AIAA Journal*.
- [10] Reddy, D.R., "3-D Navier-Stokes Analysis of Crossing, Glancing Shocks/Turbulent Boundary Layer Interactions," AIAA Paper 91-1758, June 1991.
- [11] Rubesin, M. and Rose, W., "The Turbulent Mean Flow Reynolds-Stress and Heat Flux Equations in Mass Averaged Dependent Variables," NASA TMX 62248, 1973.
- [12] Baldwin, B. and Lomax, H., "Thin Layer Approximation and Algebraic Model for Separated Turbulent Flows," AIAA Paper 78-257, 1978.
- [13] Knight, D., "A Hybrid Explicit-Implicit Numerical Algorithm for the Three Dimensional Compressible Navier-Stokes Equations," *AIAA Journal*, Vol. 22, 1984.
- [14] Knight, D.D., Horstman, C.C., and Monson, D.J., "The Hypersonic Shock Wave-Turbulent Boundary Layer Interaction Generated by a Sharp Fin at Mach 8.2," AIAA Paper 92-0747, Jan. 1992.
- [15] Knight, D.D. and Badekas, D., "On the Quasi-Conical Flowfield Structure of the Swept Shock Wave-Turbulent Boundary Layer Interaction," AIAA Paper 91-1759, June 1992.
- [16] Narayanswami, N., Knight, D.D., and Horstman, C.C., "The Investigation of a Hypersonic 3-D Crossing Shock/Turbulent Boundary Layer Interaction," submitted to *Shock Waves*.

Table 1 Grid Details

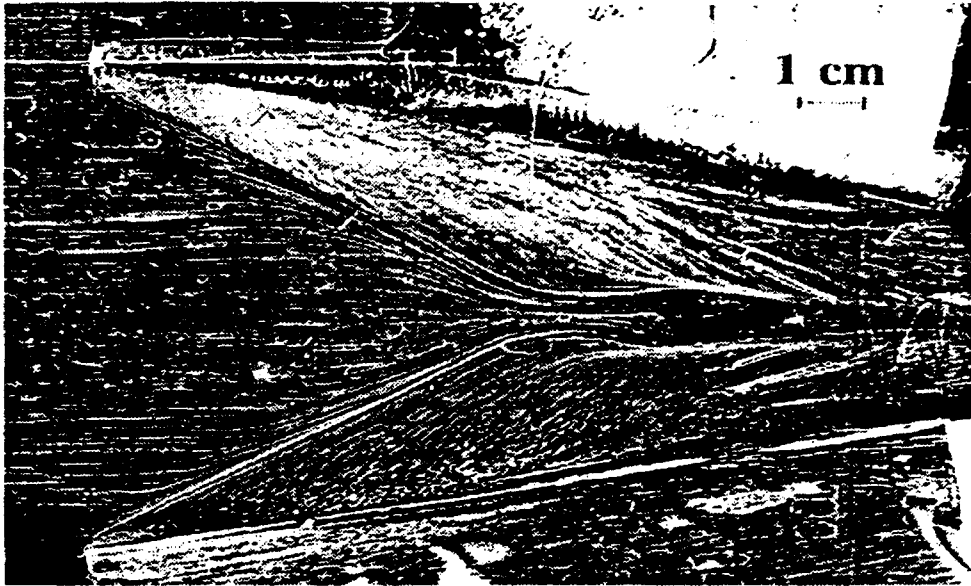
z - direction					
$N_z$	$\Delta z / \delta_\infty^\dagger$	$z_{in} / \delta_\infty$	$z_{out} / \delta_\infty$		
66	0.64	-5.0	42.2		
y - direction					
$N_y$	$\Delta y / \delta_\infty  _{min}$	$\Delta y / \delta_\infty  _{max}$	$y_{max} / \delta_\infty$	NBL	
66	$1.2 \times 10^{-4}$	0.58	22.9	28	
x - direction					
$N_x$	$\Delta x / \delta_\infty  _{min}$	$\Delta x / \delta_\infty  _{max}$	$x_{max} / \delta_\infty$	NBL	
44	$1.9 \times 10^{-4}$	0.74	13.76	20	

Legend:  $\delta$  = boundary layer thickness,  $N_z, N_y, N_x$  = number of points along z, y and x directions, respectively,  $\Delta z, \Delta y, \Delta x$  = grid spacings in the z, y and x directions, respectively, subscripts: *in, out* = at inflow, outflow planes, *max* = maximum, *min* = minimum,  $\infty$  = evaluated in freestream, symbols:  $\dagger$  = variable grid spacing, reported values are in vicinity of inviscid shock crossing location.

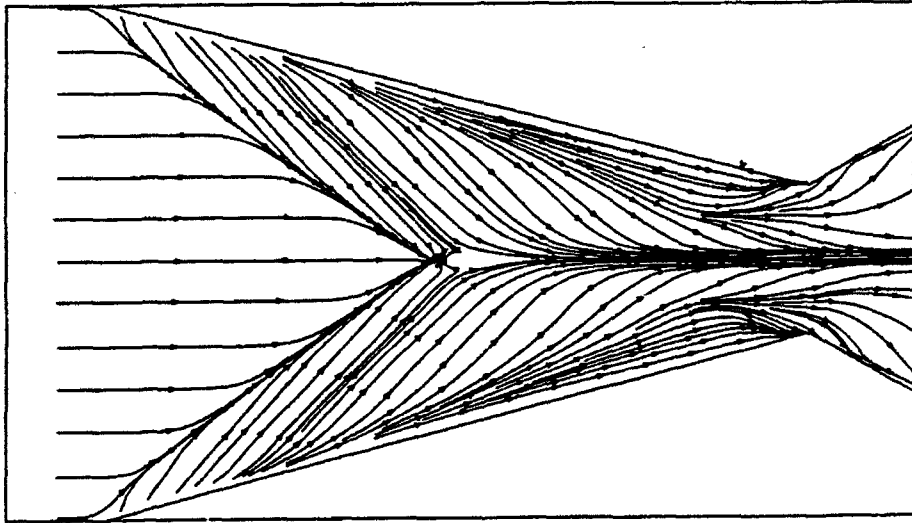


Legend:  $\alpha$  = fin angle,  $\theta$  = outflow duct angle (in computation), P = primary shock, R = reflected shock, E = expansion fan

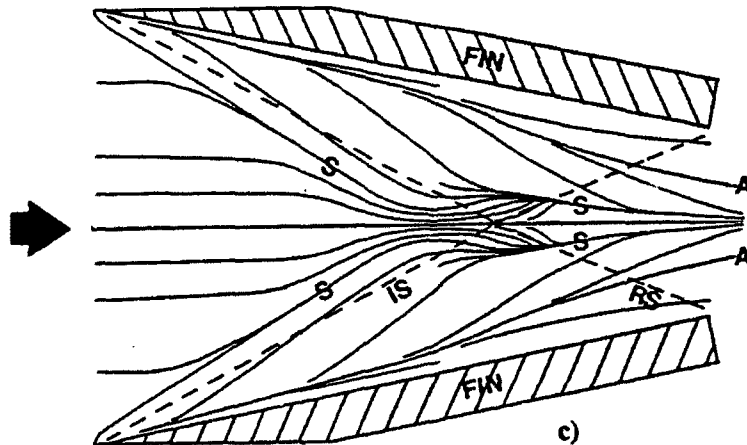
Figure 1 Model Geometry: a) perspective view of experimental geometry; b) top view of computational geometry.



a)

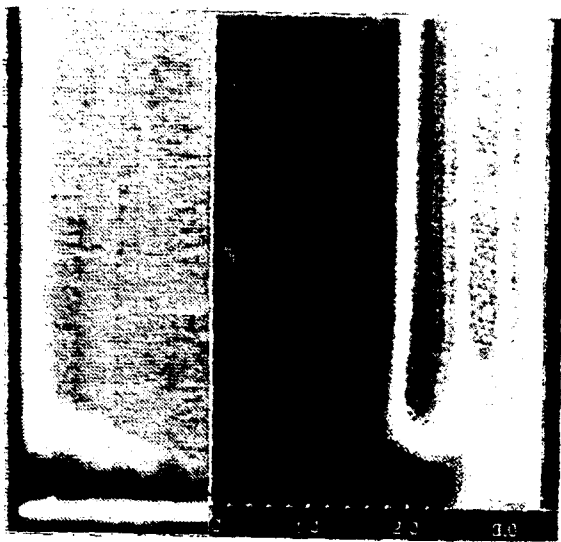


b)

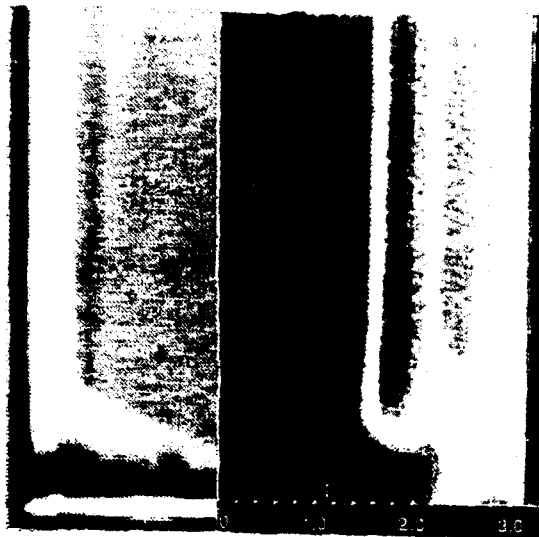


c)

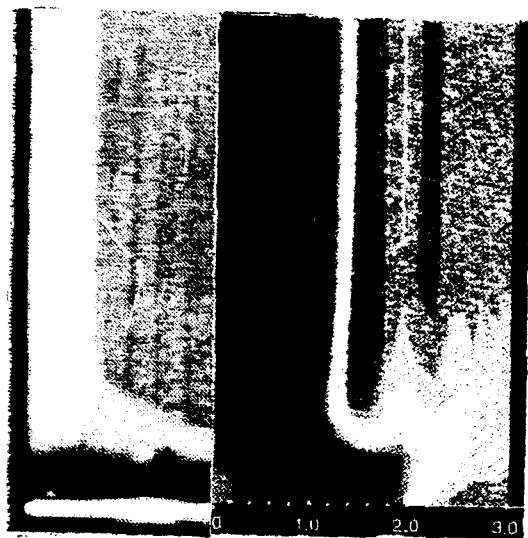
Figure 2 Surface patterns: a) experimental trace, Mach 3,  $\alpha = 11$  degrees; b) computational trace, Mach 4,  $\alpha = 15$  degrees; c) sketch showing key features.



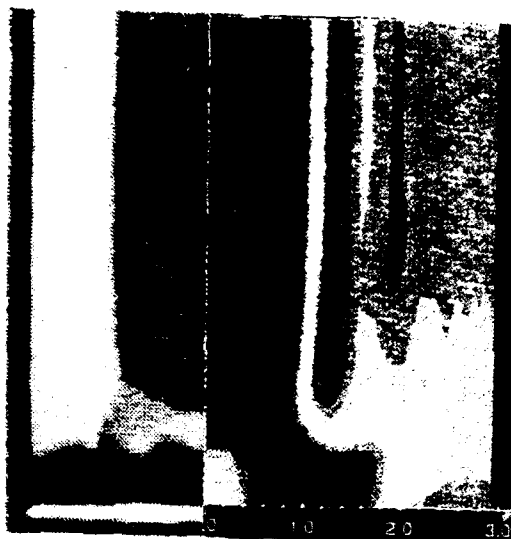
a)  $\min = 0.99, \Delta = 0.16$



b)  $\min = 0.99, \Delta = 0.16$



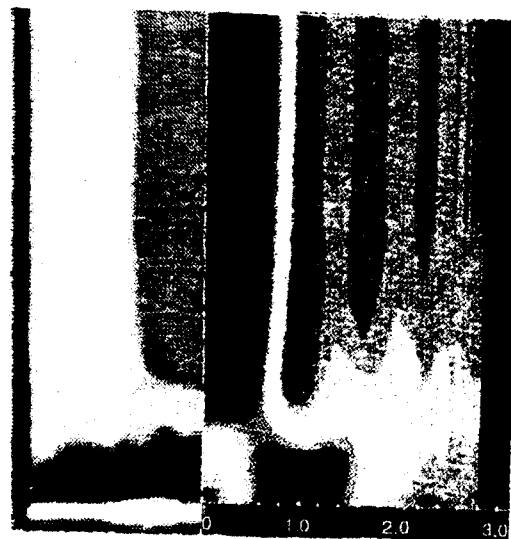
c)  $\min = 0.99, \Delta = 0.16$



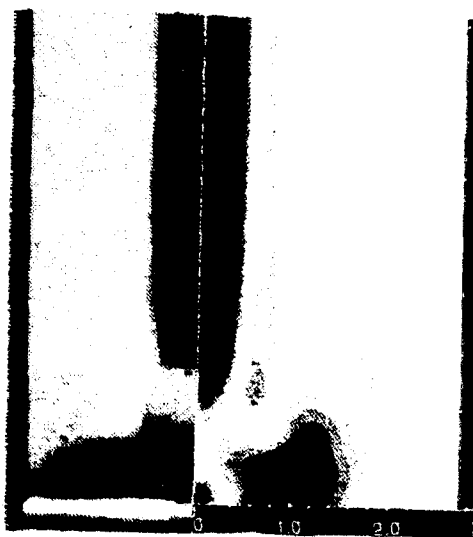
d)  $\min = 0.99, \Delta = 0.16$



KEY



e)  $\min = 0.99, \Delta = 0.15$



f)  $\min = 1.13, \Delta = 0.17$

Figure 3 Comparison of experimental PLS images with computational results



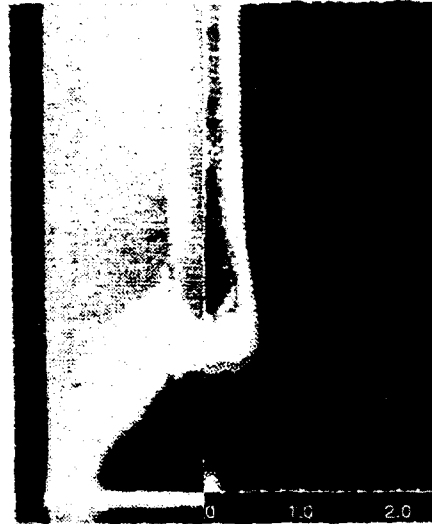
g)  $\min = 2.52, \Delta = 0.14$



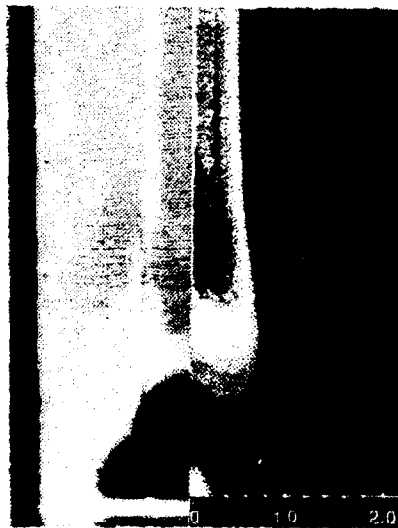
h)  $\min = 3.04, \Delta = 0.28$



i)  $\min = 3.36, \Delta = 0.35$



j)  $\min = 3.42, \Delta = 0.36$

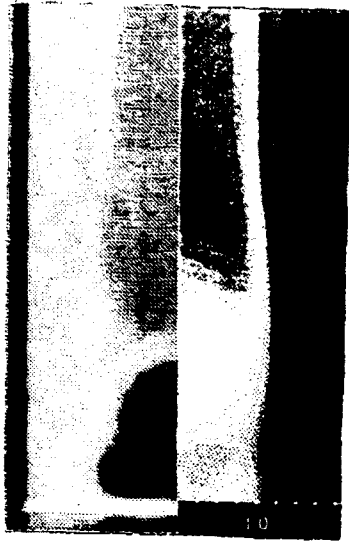


k)  $\min = 3.42, \Delta = 0.36$

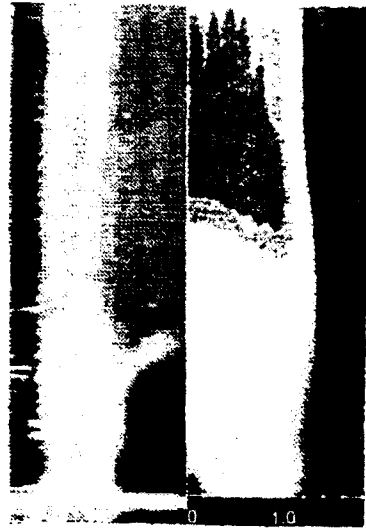


l)  $\min = 3.41, \Delta = 0.36$

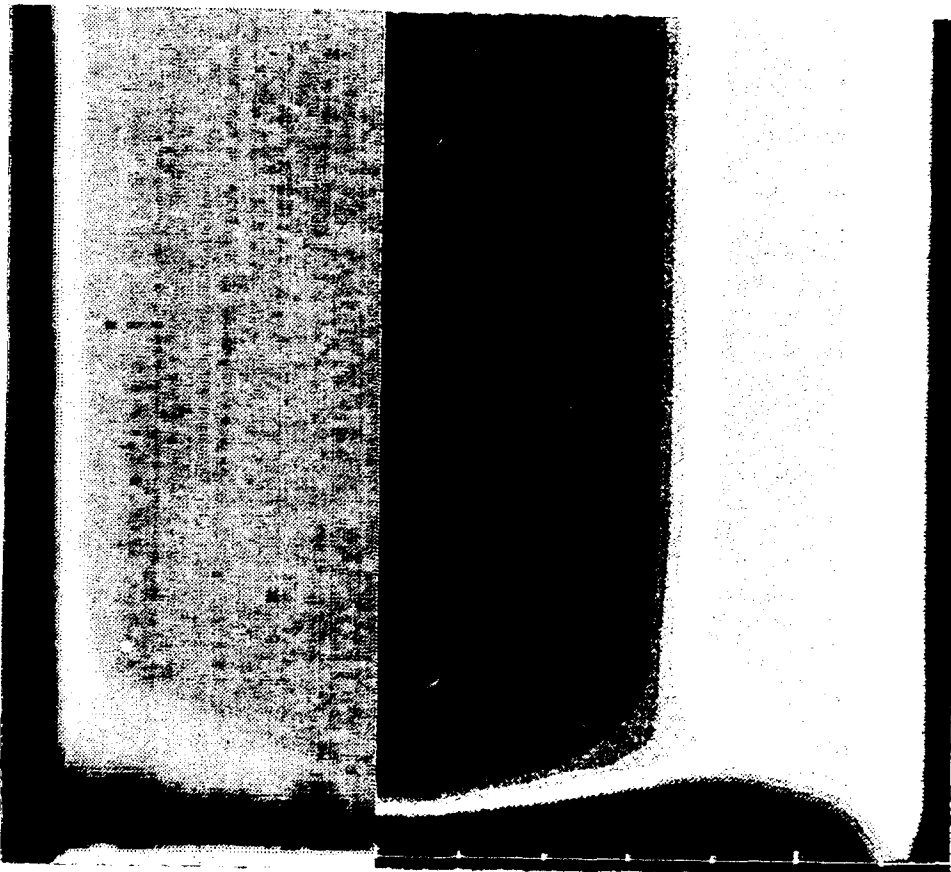
Figure 3 (continued) Comparison of experimental PLS images with computational results



m)  $\min = 3.38, \Delta = 0.36$



n)  $\min = 3.27, \Delta = 0.38$



o)  $P/P_{\min}$  at the same plane as frame a),  $\min = 0.00, \Delta = 0.15$

Figure 3 (concluded) Comparison of experimental PLS images with computational results

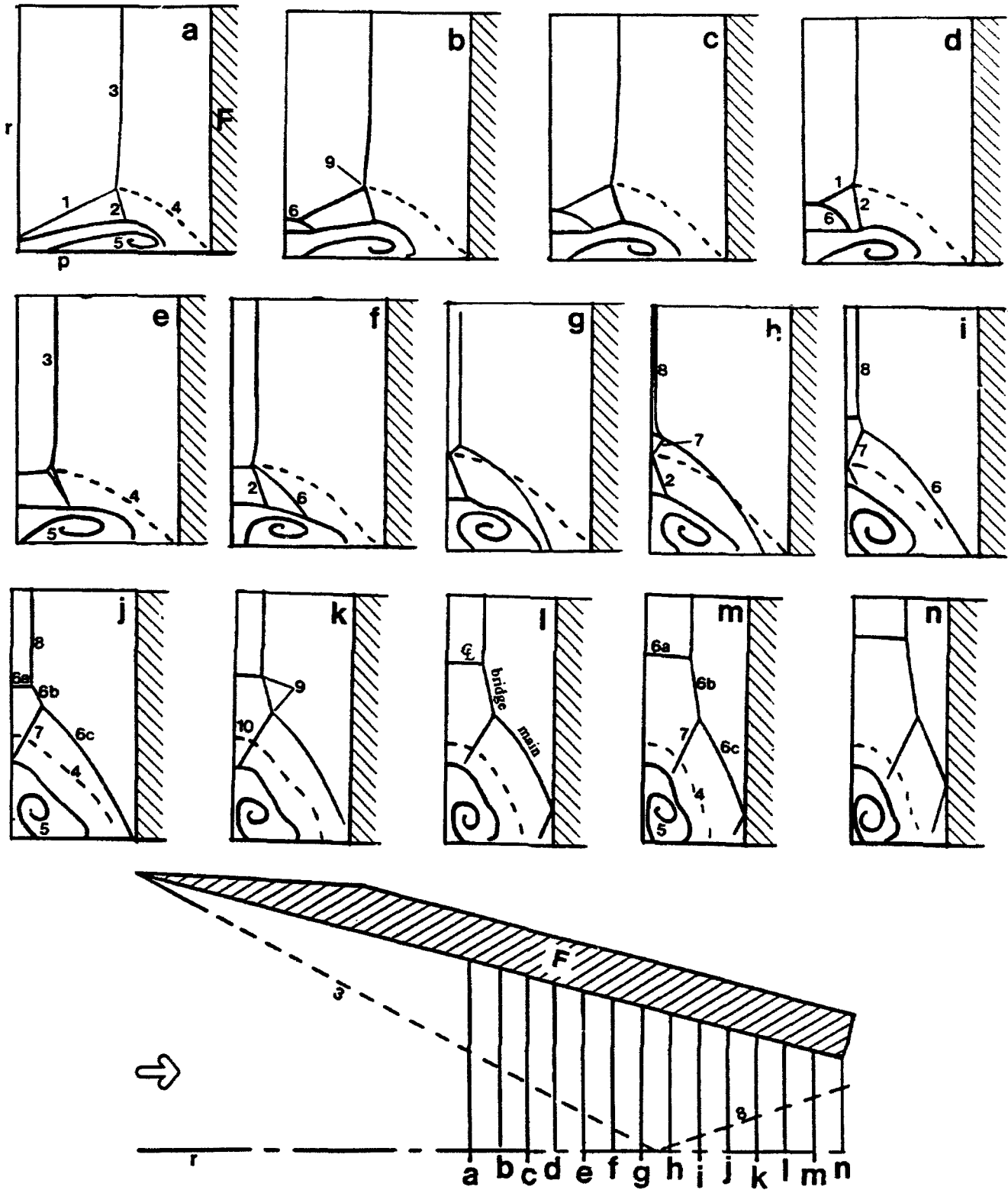


Figure 4 Flowfield diagrams corresponding to Fig. 3, for Mach 4,  $\alpha = 15$  degree interaction, with top view showing locations of planes a-n. Key: F - fin, p - flat plate, r - reflection plane (model centerline), 1 - incident separation shock, 2 - incident rear shock, 3 - incident "inviscid" shock, 4 - slip line, 5 - separation vortex, 6 - reflected separation shock (6a - centerline segment, 6b - bridge segment, 6c - main segment), 7 - reflected rear shock, 8 - reflected "inviscid shock", 9 - triple point, 10 - expansion.

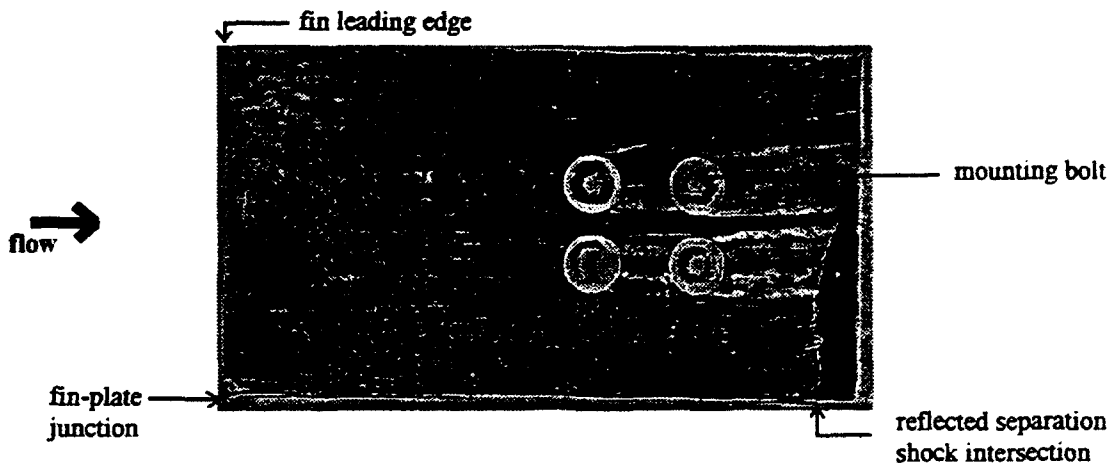


Figure 5 Fin surface flow pattern for a Mach 3, 9 degree interaction.

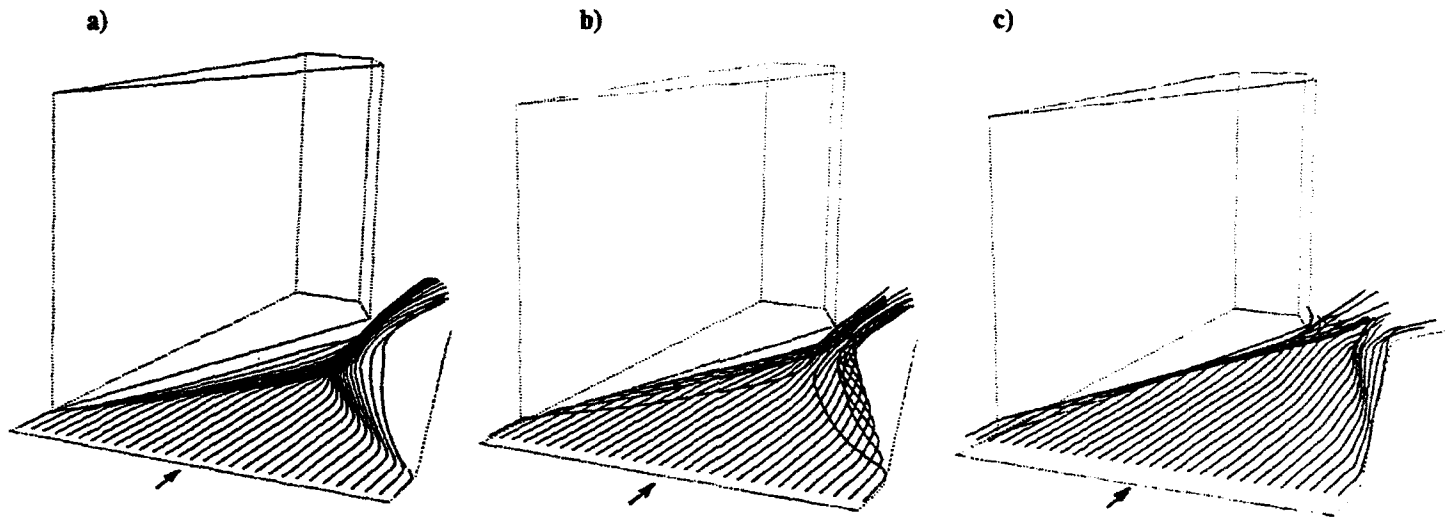


Figure 6 Particle traces: a)  $y/\delta_\infty = 0.01$ ; b)  $y/\delta_\infty = 0.25$ ; c)  $y/\delta_\infty = 1.0$ .

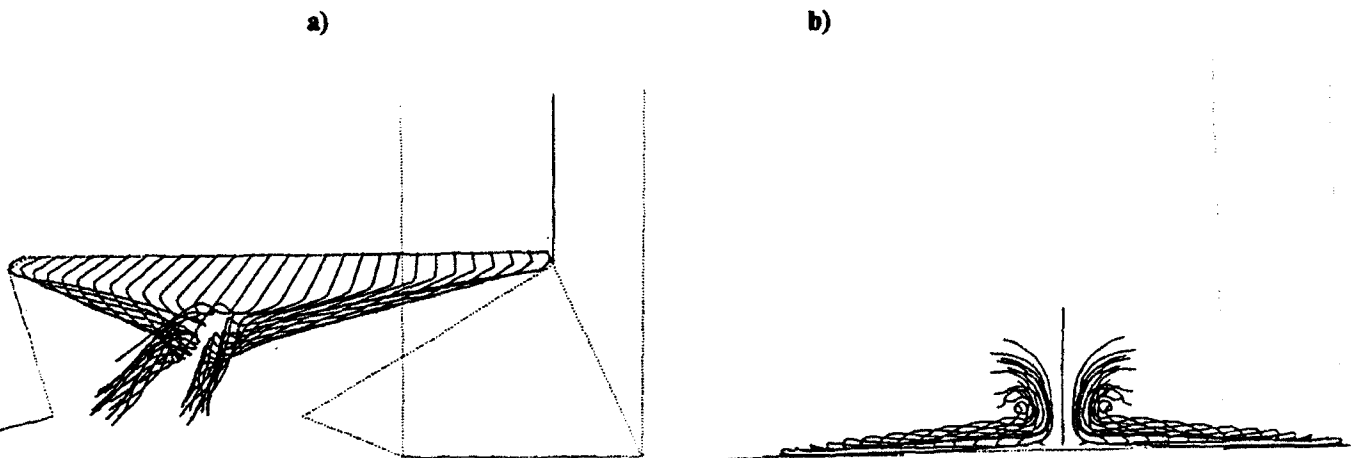


Figure 7 Downstream view of particle trace for particles originating at  $y/\delta_\infty = 0.25$ : a) perspective view; b) rear view.